Giant resonances in ^{40}Ca and ^{48}Ca

M. R. Anders, S. Shlomo, Tapas Sil, D. H. Youngblood, Y.-W. Lui, and Krishichayan

Phys. Rev. C **87**, 024303 — Published 6 February 2013

DOI: 10.1103/PhysRevC.87.024303

Giant resonances in ^{40}Ca and ^{48}Ca

M. R. Anders[1], S. Shlomo[1], Tapas Sil[1,2], D.H. Youngblood[1], Y.-W. Lui[1] and Krishichayan[1,3]

[1]Cyclotron Institute, Texas A&M University, College Station, Texas 77843

[2]Indian Institute of Information Technology Design and Manufacturing, Kancheepuram, Chennai 600 127, Tamil Nadu, India.

[3]Dept. of Pure and Applied Physics, Guru Ghasidas University Bilaspur-495009 C G India

We present results of fully self-consistent Hartree-Fock based random phase approximation calculations of the strength functions S(E) and centroid energies E_{CEN} of isoscalar ($T = 0$) and isovector ($T = 1$) giant resonances of multipolarities $L = 0$ - 3 in ^{40}Ca and ^{48}Ca, using a wide range of commonly employed 18 Skyrme type nucleon-nucleon effective interactions. We determined the sensitivities of E_{CEN} and of the isotopic differences $E_{CEN}(^{48}Ca)$ - $E_{CEN}(^{40}Ca)$ to physical quantities, such as nuclear matter incompressibility coefficient, symmetry energy density and effective mass, associated with the Skyrme interactions and compare the results with the available experimental data.

PACS numbers: 24.30.Cz, 21.60.Jz, 21.65.-f

1. Introduction

The study of collective modes in nuclei has been the subject of extensive theoretical and experimental studies during several decades [1-3], since it contributes significantly to our understanding of bulk properties of nuclei, their non-equilibrium properties and properties of the nuclear force. Of particular interest is the equation of state (EOS), i.e. the binding energy per nucleon as a function of the neutron (N) and proton (Z) densities, of infinite nuclear matter (no Coulomb interaction). The EOS is an important ingredient in the study of properties of nuclei at and away from stability, the study of structure and evolution of compact astrophysical objects, such as neutron stars and core-collapse supernovae, and the study of heavy-ion collisions (HIC) [4,5]. The saturation point of the equation of state (EOS) for symmetric (N=Z) nuclear matter (NM) is well determined from the measured binding energies and central matter densities of nuclei, by extrapolation to infinite NM [1,2]. To extend our knowledge of the EOS beyond the saturation point of symmetric NM, an accurate value of the NM incompressibility coefficient K_{NM}, which is directly related to the curvature of the EOS of symmetric NM, is needed. An accurate knowledge of the dependence of the symmetry energy, $E_{sym}(\rho)$, on the matter density ρ is needed for the EOS of asymmetric NM.

There have been many attempts over the years to determine K_{NM} and $E_{sym}(\rho)$ by considering physical quantities which are sensitive to the values of K_{NM} and $E_{sym}(\rho)$ [3,4,6,7]. In this work we investigate the sensitivity of the strength function distributions of the isoscalar and isovector giant resonances with multipolarities L = 0-3 of the isotopes ^{40}Ca and ^{48}Ca to bulk properties of NM, such as K_{NM}, E_{sym} and the effective mass m*. It is well known that the energies of the compression modes, the isoscalar giant monopole

resonance (ISGMR) and isoscalar giant dipole resonance (ISGDR), are very sensitive to the value of K_{NM} [1,3,8]. Also the energies of the isovector giant resonances, in particular, the isovector giant dipole resonance (IVGDR), are sensitive to the density dependence of E_{sym} [9,10], commonly parameterized in terms of the quantities J, L and K_{sym}, which are the value of $E_{sym}(\rho)$ at saturation density (also known as symmetry energy coefficient), and the quantities directly related to the derivative and the curvature of $E_{sym}(\rho)$ at the saturation density, respectively. Furthermore, information on the density dependence of E_{sym} can also be obtained by studying the isotopic dependence of strength functions, such as the difference between the strength functions of ^{40}Ca and ^{48}Ca and between ^{112}Sn and ^{124}Sn. We note that the value of the neutron-proton asymmetry parameter $\delta = (N-Z)/A$ increases from ^{40}Ca to ^{48}Ca by a value of 0.167 which is significantly larger than the change of 0.087 between ^{112}Sn and ^{124}Sn.

In early analysis of the experimental data on the ISGMR [11,12], a semiclassical model was adopted in order to relate the energy of the ISGMR to an incompressibility coefficient K_A of the nucleus and carry out a Leptodermous ($A^{-1/3}$) expansion of K_A, similar to a mass formula, to parameterize K_A into volume (K_{NM}), surface (K_S), symmetry (K_τ) and coulomb (K_C) terms [11,13,14]. Shlomo and Youngblood [14] showed that this type of analysis could not provide a unique solution even including all available world data as of that time. More recently [15] a semiclassical analysis of the ISGMR data in the Sn isotopes demonstrated that the value obtained for K_τ is quite sensitive to the number of terms employed in the Leptodermous expansion. In this work we adopt the microscopic approach of fully self consistent Hartree-Fock (HF) based random phase approximation (RPA), employing an effective nucleon-nucleon interaction. In the HF-RPA approach,

the values of K_{NM} and the density dependence of E_{sym} are then deduced from the interaction that best reproduces the experimental data on the strength functions of the giant resonance. (see the review in Ref. [3]). It is important to note that ground state properties of nuclei are well described by the HF approximation, using an effective nucleon-nucleon interaction, such as the Skyrme type interaction [16-18], with parameters obtained by a fit to a selected set of experimental data on binding energies and radii of nuclei [1,2]. It has also been demonstrated that HF-based RPA nicely reproduces the properties of low lying collective states as well as of giant resonances [1,2].

Recently the giant resonance region from 9.5 MeV < E_x < 40 MeV in ^{48}Ca was studied with inelastic scattering of 240 MeV α particles at small angles, including 0º. Close to 100% of the ISGMR (E0), ISGDR (E1) and isoscalar giant quadrupole resonance (E2) strengths have been located between 9.5 and 40 MeV in ^{48}Ca [19]. To study the effect of neutron-proton asymmetry, a comparison with the available data for ^{40}Ca [20-22], as well as with the results obtained within the HF-based RPA, was carried out in Ref. [19]. The ISGMR has been found at somewhat higher energy in ^{48}Ca than in ^{40}Ca, whereas self consistent HF-RPA calculations obtained using the SGII [23], KDE0 [24], SKM* [25] and SK255 [26] Skyrme interactions predict a centroid energy in this neutron rich Ca isotope lower than in ^{40}Ca .

In this work we extend our theoretical investigation by considering the isoscalar and isovector giant resonances of multipolarities $L = 0 - 3$ in ^{40}Ca and ^{48}Ca. In the next section we review the basic elements of the self-consistent HF-based RPA theory for the strength functions of isoscalar ($T = 0$) and isovector ($T = 1$) giant resonances. In section 3

we present results of our calculations for the strength functions S(E) and centroid energies E_{CEN} obtained for giant resonances of *T = 0, 1* and multipolarities *L = 0 - 3* in ^{40}Ca and ^{48}Ca, using a wide range of 18 commonly used Skyrme type nucleon-nucleon effective interactions. We pay attention to the issue of self-consistency and investigate the sensitivities of E_{CEN} and of the isotopic differences $E_{CEN}(^{48}Ca) - E_{CEN}(^{40}Ca)$ to physical quantities, such as nuclear matter incompressibility coefficient, symmetry energy density and effective mass, associated with the effective nucleon-nucleon interactions, and compare the results with available experimental data. In the last section, we discuss our results and present our conclusions.

2. Self-consistent HF based RPA Approach

In numerical calculations of the properties of giant resonances in nuclei within the HF-based RPA theory, one starts by adopting an effective nucleon-nucleon interaction V_{12}, such as the Skyrme interaction, with parameters determined by a fit of the HF predictions to experimental data on ground state properties, such as binding energies and radii, of a selected set of a wide range of nuclei. Then, the RPA equations are solved using the particle-hole interaction deduced from V_{12}, by employing a certain numerical method [27-29], and the physical quantities of interest, such as the strength functions S(E) and transition densities, are calculated. We point out that in a fully self-consistent HF-based RPA calculations, one should include all the components of V_{12} in the RPA calculations and use a sufficiently large particle-hole configuration space to insure convergence. Necessary conditions for fully self consistent calculations are; (i) The

spurious isoscalar dipole state (due to center of mass motion) is obtained at zero energy; and (ii) The energy weighted sun rules (EWSR) are fulfilled.

2.1 Skyrme Energy Density Functional

In our calculations we have adopted the following form for the Skyrme type effective nucleon-nucleon interaction [30]:

$$V_{12} = t_0(1 + x_0P_{12}^{\sigma})\delta(\vec{r}_1 - \vec{r}_2) + \frac{1}{2}t_0(1 + x_1P_{12}^{\sigma})\left[\overleftarrow{k}_{12}^2\delta(\vec{r}_1 - \vec{r}_2) + \delta(\vec{r}_1 - \vec{r}_2)\vec{k}_{12}^2\right]$$
$$+ t_2(1 + x_2P_{12}^{\sigma})\overleftarrow{k}_{12}\delta(\vec{r}_1 - \vec{r}_2)\vec{k}_{12} + \frac{1}{6}t_3(1 + x_3P_{12}^{\sigma})\rho^{\alpha}\left(\frac{\vec{r}_1+\vec{r}_2}{2}\right)\delta(\vec{r}_1 - \vec{r}_2) \quad (1)$$
$$+iW_0\overleftarrow{k}_{12}\delta(\vec{r}_1 - \vec{r}_2)(\vec{\sigma}_1 + \vec{\sigma}_2) \times \vec{k}_{12} ,$$

where t_i, x_i, α, and W_0 are the parameters of the interaction and P_{12}^{σ} is the spin exchange operator, $\vec{\sigma}_i$ is the Pauli spin operator, $\vec{k}_{12} = -i\left(\vec{\nabla}_1 - \vec{\nabla}_2\right)/2$, and $\overleftarrow{k}_{12} = -i\left(\overleftarrow{\nabla}_1 - \overleftarrow{\nabla}_2\right)/2$. Here, the right and left arrows indicate that the momentum operators act on the right and on the left, respectively. The corresponding mean-field V_{HF} and the total energy E of the system are given by

$$V_{HF} = \frac{\delta H}{\delta \rho}, \qquad E = \int H(r)\, d^3r, \quad (2)$$

respectively, where $H(r)$ is the Skyrme energy-density functional [31], obtained using Eq. (1). It is given by [30],

$$H = K + H_0 + H_3 + H_{eff} + H_{fin} + H_{so} + H_{sg} + H_{Coul} , \quad (3)$$

where,

$$K = \frac{\hbar^2}{2m}\tau , \quad (4)$$

is the kinetic-energy term. For the Skyrme interaction of Eq. (1), we have

$$H_0 = \frac{1}{4}t_0\left[(2+x_0)\rho^2 - (2x_0+1)\left(\rho_p^2+\rho_n^2\right)\right], \tag{5}$$

$$H_3 = \frac{1}{24}t_3\rho^\alpha\left[(2+x_3)\rho^2 - (2x_3+1)\left(\rho_p^2+\rho_n^2\right)\right], \tag{6}$$

$$H_{eff} = \frac{1}{8}[t_1(2+x_1)+t_2(2+x_2)]\tau\rho + \frac{1}{8}[t_2(2x_2+1)-t_1(2x_1+1)]\left(\tau_p\rho_p+\tau_n\rho_n\right), \tag{7}$$

$$H_{fin} = \frac{1}{32}[3t_1(2+x_1)-t_2(2+x_2)](\nabla\rho)^2 - \frac{1}{32}[3t_1(2x_1+1)+t_2(2x_2+1)]\left[\left(\nabla\rho_p\right)^2+(\nabla\rho_n)^2\right], \tag{8}$$

$$H_{so} = \frac{W_0}{2}\left[J\cdot\nabla\rho + x_w\left(J_p\cdot\nabla\rho_p + J_n\cdot\nabla\rho_n\right)\right], \tag{9}$$

and

$$H_{sg} = -\frac{1}{16}(t_1x_1+t_2x_2)J^2 + \frac{1}{16}(t_1-t_2)\left(J_p^2+J_n^2\right). \tag{10}$$

Here, H_0 is the zero-range term, H_3 is the density dependent term, H_{eff} is an effective-mass term, H_{fin} is a finite-range term, H_{so} is a spin-orbit term, H_{sg} is a term that is due to tensor coupling with spin and gradient and H_{Coul} is the contribution to the energy-density that is due to the Coulomb interaction. In Eqs. (5) – (10) $\rho = \rho_p + \rho_n$, $\tau = \tau_p + \tau_n$, and $J = J_p + J_n$, are the particle number density, kinetic-energy density and spin-density with p and n denoting the protons and neutrons, respectively [30]. Note that the additional parameter x_w, introduced in Eq. (9), allows us to modify the isospin dependence of the spin-orbit term.

The contribution to the energy-density, Eq. (3), from the Coulomb interaction can be written as a sum of a direct and an exchange terms:

$$H_{Coul}(r) = H_{Coul}^{dir}(r) + H_{Coul}^{ex}(r). \tag{11}$$

For the direct term it is common to adopt the expression

$$H_{Coul}^{dir}(r) = \frac{1}{2}e^2\rho_p(r)\int\frac{\rho_p(r')}{|r-r'|}d^3r' \ , \tag{12}$$

and for the corresponding exchange term to use the Slater approximation

$$H_{Coul}^{ex}(r) = -\frac{3}{4}e^2\rho_p(r)\left[\frac{3\rho_p(r)}{\pi}\right]^{1/3} \ . \tag{13}$$

It is very important to emphasize that the definitions of Eqs. (12) and (13) are not for the bona fide direct and exchange terms since each of them includes the contributions of the self-interaction term, which appear in opposite signs and cancel out in Eq. (11), see Ref. [32].

The HF approach applied to finite nuclei violates translational invariance, introducing a spurious center of mass (CM) motion. Thus, one must extract the contributions of the CM motion to the binding energy B, rms radii and other observables. To account for the CM correction to the total binding energy, one must subtract from it the so-called CM energy given as,

$$E_{CM} = \frac{1}{2mA}\langle\hat{P}^2\rangle \ , \tag{14}$$

where, $P = -i\hbar\sum_i\nabla_i$ is the total linear momentum operator.

During the last four decades, many Skyrme type effective nucleon-nucleon interactions of different forms were obtained by fitting the HF results to selected sets of experimental data [33,34]. We emphasize that in this work we consider the specific form of Eq. (1) for the Skyrme type interaction. The values of the Skyrme parameters of the interactions adopted in this work are listed in Table 1. It is very important to note that in determining the parameters of the Skyrme interaction, Eq. (1), several approximations, concerning the terms of Eqs. (4), (10), (11) and (14), were made in the HF calculations.

These approximations, which should be taken into account for a proper application of the specific interaction in fully self-consistent HF based RPA calculations, are:

(i) **The kinetic term, Eq. (4)**. In some interactions the mass of the proton is taken to be equal to that of the neutron and a certain value for the nucleon mass is adopted. In other interactions the mass of the proton is taken to be different than that of the neutron.

(ii) **The spin-density terms, Eq**. **(10)**. In some interactions the contributions from the spin-density term as given by Eq. (10), are ignored. We note that contributions from Eq. (10) are crucial for the calculation of the Landau parameter $G_0^{'}$.

(iii) **The Coulomb term, Eq**. **(11)**. In some interactions the Coulomb term of Eq. (13) is omitted. It is important to note that by neglecting the term of Eq. (13), one neglects the bona fide Coulomb exchange term together with the spurious contribution of the self-interaction term. This leads to a contribution to Coulomb displacement energies, obtained from Eq. (12), which is in better agreement with experimental data [35], since in the HF calculations with Skyrme interactions one neglects the contributions due to charge symmetry breaking in the nucleon-nucleon interaction and the contribution to Coulomb energy associated with long range correlations. Also, in some interactions the charge density is used in Eq. (11), instead of the point proton density.

(iv) **The center of mass correction, Eq. (14)**. Traditionally, one simplifies the computation of Eq. (14) by taking into account only the one-body parts of it, which can be easily achieved by replacing $\frac{1}{m} \rightarrow \frac{1}{m}\left[1-\frac{1}{A}\right]$ in the kinetic-

energy term. In this case, the effects of neglecting the two-body part of Eq. (14) are compensated by renormalization of the force parameters. This may induce in the forces an incorrect trend with respect to the nucleon number A that becomes visible in the nuclear matter properties. A more appropriate approach, used in some interactions, is to take into account the contribution of the two body terms by using the HF single particle wavefunctions or by employing a simple scheme to evaluate Eq. (14).

The approximations that were used to obtain the Skyrme interactions adopted in this work are listed for each interaction in Table 2.

2.2 RPA calculations of strength functions

In this work we have carried out fully self-consistent HF-based RPA calculations for electric giant resonances in ^{40}Ca and ^{48}Ca using the effective energy density functionals (EDF) given by Eqs. (3) to (14) with Tables 1 and 2 and employing the numerical method for RPA described in Ref. [28,36,37], which is formulated in terms of coordinate like Q (time-even) and momentum like P (time-odd) particle-hole (p-h) operators and adapted for a given EDF. We point out that in order to insure self-consistency we have carried out the calculations using a large p-h space and included all the terms of the p-h residual interaction (time-even and time-odd) which are associated with the EDF used in the HF calculations. No additional time-odd residual interactions were added. For a given scattering operator F_L, we have calculated the strength function

$$S(E) = \sum_j |\langle 0|F_L|j\rangle|^2 \delta\left(E_j - E_0\right). \quad (15)$$

Here, $|0\rangle$ is the RPA ground state and the sum is over all RPA excited states $|j\rangle$ with the corresponding excitation energies E_j. We adopt the single particle scattering operator

$$F_L = \sum_i f(r_i) Y_{L0}(i) \ , \tag{16}$$

for isocalar ($T = 0$) excitations and

$$F_L = \frac{Z}{A}\sum_n f(r_n) Y_{L0}(n) - \frac{N}{A}\sum_p f(r_p) Y_{L0}(p) \ , \tag{17}$$

for isovector excitations ($T = 1$). In Eqs. (16) and (17) we use the operator $f(r) = r$, for the isovector dipole ($T = 1$, $L = 1$) and $f(r) = r^3 - (5/3)\langle r^2 \rangle r$ for the isoscalar dipole ($T = 0$, $L = 1$), to eliminate possible contribution of the spurious state mixing [38,39]. For the isoscalar and isovector monopole ($L = 0$), quadrupole ($L = 2$) and octopole (L=3) excitations we use the operators r^2, r^2, and r^3, respectively. We then determine the energy moments of the strength function,

$$m_k = \int_0^\infty E^k S(E)\, dE \ . \tag{18}$$

The centroid energy, E_{CEN}, is then obtained from

$$\mathrm{E_{CEN}} = \frac{m_1}{m_0} \ . \tag{19}$$

The energy moment m_1 can also be calculated using the HF ground state wave function, thereby leading to an energy weighted sum rule (EWSR) [1, 10]. For the isoscalar F_L in Eq. (16), the EWSR is given by,

$$m_1(L, T = 0) = \frac{1}{4\pi}\frac{\hbar^2}{2m}\int g_L(r)\, \rho(r) 4\pi r^2 dr \ , \tag{20}$$

where $\rho(r)$ is the HF ground-state matter density distribution and

$$g_L(r) = \left(\frac{df}{dr}\right)^2 + L(L+1)\left(\frac{f}{r}\right)^2 \ . \tag{21}$$

For the isovector (T=1) operator F_L of Eq. (17), the EWSR is given by

$$m_1(L, T = 1) = \frac{NZ}{A^2} m_1(L, T = 0)\left[1 + \kappa - \kappa_{np}\right] , \tag{22}$$

where κ is the enhancement factor which is due to the momentum dependence of the effective nucleon-nucleon interaction and is given by

$$\kappa = \frac{(1/2)[t_1(1+x_1/2)+t_2(1+x_1/2)]}{(\hbar^2/2m)(4NZ/A^2)} \times$$

$$\frac{2\int g_L(r)\rho_p(r)\rho_n(r)4\pi r^2 dr}{\int g_L(r)\rho(r)4\pi r^2 dr} \quad , \tag{23}$$

where t_i and x_i are the parameters of the Skyrme interaction. The correction κ_{np}, which arises because of the difference in the profiles of the neutron and proton density distributions [i.e., because $\rho_n(r) - \rho_p(r) \neq \frac{N-Z}{A}\rho(r)$], is given by

$$\kappa_{np} = \frac{(N-Z)}{A}\frac{A}{NZ}\frac{\int g_L(r)[Z\rho_n(r)-N\rho_p(r)]4\pi r^2 dr}{\int g_L(r)\rho(r)4\pi r^2 dr} \, . \tag{24}$$

We have carried out fully self-consistent Hartree-Fock (HF) based RPA calculations of the isoscalar giant monopole resonance (ISGMR), dipole (ISGDR), quadrupole (ISGQR), and the octopole (ISGOR) strength functions, adopting the scattering operator of Eq. (16), and for the isovector giant monopole resonance (IVGMR), dipole (IVGDR), quadrupole (IVGQR) and octopole (IVGOR) strength functions, adopting the scattering operator of Eq. (17), for ^{40}Ca and for ^{48}Ca, using a wide range of 18 Skyrme type effective interactions (Table 1). In the next section we present the results of our calculations and compare with available experimental data**.**

2.3 Equation of state of nuclear matter

In the vicinity of the saturation density ρ_0 of symmetric NM, the EOS can be approximated by

$$\mathrm{E_0[\rho]} = \mathrm{E[\rho_0]} + \frac{1}{18}\mathrm{K_{NM}}\left(\frac{\rho-\rho_0}{\rho_0}\right)^2, \tag{25}$$

where $E_0[\rho]$ is the binding energy per nucleon and K_{NM} is the incompressibility coefficient which is directly related to the curvature of the EOS, $K_{NM} = 9\rho_0^2 \frac{\partial^2 E_0}{\partial \rho^2}\Big|_{\rho_0}$. Similarly, the EOS of asymmetric NM, with proton density ρ_p and neutron density ρ_n, can be approximated by

$$E[\rho_p, \rho_n] = E_0[\rho] + E_{sym}[\rho]\left(\frac{\rho_n - \rho_p}{\rho}\right)^2, \tag{26}$$

where $E_{sym}[\rho]$ is the symmetry energy at matter density ρ, approximated as

$$E_{sym}[\rho] = J + \frac{1}{3}L\left(\frac{\rho-\rho_0}{\rho_0}\right) + \frac{1}{18}K_{sym}\left(\frac{\rho-\rho_0}{\rho_0}\right)^2, \tag{27}$$

where $J = E_{sym}[\rho_0]$ is the symmetry energy at saturation density ρ_0, $L = 3\rho_0 \frac{\partial E_{sym}}{\partial \rho}\Big|_{\rho_0}$, and $K_{sym} = 9\rho_0 \frac{\partial^2 E_{sym}}{\partial \rho^2}\Big|_{\rho_0}$.

Table 3 contains the values of the physical quantities of symmetric nuclear matter associated with these Skyrme interactions: the binding energy per nucleon E/A, the saturation matter density ρ_0, the effective mass m*/m, the incompressibility coefficient of SNM, K_{NM}, the coefficients associated with the symmetry energy density J, L and K_{sym} at saturation density ρ_0 (Eq. (27)) and κ, the NM value of the enhancement factor of the EWSR of the IVGDR, Eqs (22), obtained from (23) with using the NM saturation matter density.

3. Results

We now present results of our fully self-consistent HF based RPA calculations of the strength functions and centroid energies of isoscalar and isovector giant resonances of multipolarities L = 0 - 3 in ^{40}Ca and ^{48}Ca, obtained for 18 widely used Skyrme type

interactions shown in Table 1: SGII [23], KDE0 [24], KDE0v1 [24], SKM* [25], SK255 [26], SkI3 [40], SkI4 [40], SkI5 [40], SV-bas [41], SV-min [41], SV-m56-O [42], SV-m64-O [42], SLy4 [43], SLy5 [43], SLy6 [43], SkMP [44], SkP [45], and SkO' [46]. These interactions are associated with the ranges of NM properties (see Table 3): E/A = 15.56 – 16.33 MeV, ρ_0 = 0.156 - 0.165 fm^{-3}, K_{NM} = 201 – 258 MeV, J = 26.80 – 37.40 MeV, L = 31 – 129 MeV, K_{sym} = -267 – 160 MeV, m*/m = 0.56 – 1.00 and κ = 0.08 – 0.71.

In Figures 1-4 we display the HF-based RPA results (solid lines) for the distribution of the energy-weighted strength normalized to one (ES(E)/EWSR) for the isoscalar and isovector giant resonances of multipolarities L = 0-3 in ^{40}Ca and ^{48}Ca, obtained using the KDE0 [24] interaction that is representative of the strength distributions for the rest of the interactions. For the purpose of comparison with experiment a Lorenzian smearing of a 3 MeV width was used in the calculation. The experimental data [19,21] are shown as histograms.

To investigate the sensitivity of the energies of the giant resonances in ^{40}Ca and ^{48}Ca to NM properties (Table 3) we calculated the Pearson correlation coefficients (a measure of linear correlation) between the centroid energies E_{CEN}, Eq. (19), and the properties of NM. We used a small smearing width (0.05 MeV) to insure accuracy for E_{CEN}. For a proper comparison with experiment, we used the experimental excitation energy ranges in determining the centroid energies. We use the excitation energy range of 9.5 – 40 MeV [19,21] for the ISGMR and the ISGQR and the range of 20 – 40 MeV [19,21] for the ISGDR. For the ISGOR we use the appropriate excitation energy range of 20 – 60 MeV. We use the excitation energy range of 0 – 60 MeV for the IVGMR [10,47],

the range of 0 – 40 MeV for the IVGDR [48,49,50], the range of 9 – 60 MeV for the IVGQR [51] and the range of 25 – 60 MeV for the IVGOR (see also Figures 1-4).

ISGMR

In Figure 5 we compare the experimental data [19,21] of the ISGMR centroid energies of ^{40}Ca (a), ^{48}Ca (b), and the energy difference, $\Delta E_{CEN} = E_{CEN}(^{48}Ca) - E_{CEN}(^{40}Ca)$, between ^{48}Ca and ^{40}Ca (c) with the results of fully self-consistent HF-based RPA calculations (full circles), obtained using the 18 Skyrme interactions of Table 1. The results obtained with violation of self-consistency, by the neglecting the Coulomb and the spin orbit particle-hole interactions in the RPA calculations, are shown in Fig. 5d. The calculated values are plotted as a function of K_{NM}. The experimental values of E_{CEN} = 19.18 +/- 0.37 MeV for ^{40}Ca, E_{CEN} = 19.88 +/- 0.16 MeV for ^{48}Ca [19,21] and their difference are shown in Figure 5 as the regions between the dashed lines. A very strong correlation between E_{CEN} of ^{40}Ca and E_{CEN} of ^{48}Ca can be seen with K_{NM}. This is expected, since the ISGMR centroid energy is very sensitive to the value of K_{NM} [1,3,8]. The ISGMR centroid energies for ^{40}Ca are all higher than the experimental value 19.18 +/- 0.37 MeV. The ^{48}Ca ISGMR centroid energies are more consistent with the experimental value 19.88 +/- 0.16 MeV. While the experimental data show that the ISGMR in ^{40}Ca lies at lower energy than in ^{48}Ca, 17 of the Skyrme interactions (Table 1) show the ISGMR in ^{40}Ca at a higher energy than in ^{48}Ca, while the 18th interaction (SkI3) shows them at essentially the same energy in ^{40}Ca and ^{48}Ca. For not fully self-consistent RPA calculations, the results for some interactions leads to spurious agreement with the experimental data for the ^{48}Ca – ^{40}Ca energy difference as can be seen in Fig. 5d. We also found a medium correlation between the ISGMR energies and the effective mass m*/m,

which is a reflection of the strong correlation between K_{NM} and m*/m seen in Figure 6 (see also Ref. [8]). Figure 6 also shows the correlation of the saturation symmetric NM density ρ_0 and the symmetry energy coefficient J with K_{NM} .

To investigate the dependence of the energy difference $\Delta E_{CEN} = E_{CEN}(^{48}Ca) - E_{CEN}(^{40}Ca)$ between the ISGMR in ^{48}Ca and in ^{40}Ca on the symmetry energy density, Figure 7 shows the results of our fully self-consistent HF based RPA calculations (full circles), using the Skyrme interactions (Table 1) having nuclear matter symmetry energy coefficient J = 26.80 –36.7 MeV. No correlation is found between ΔE_{CEN} and J. Similar results were obtained for L, K_{sym} and K_{NM}, which can be easily understood as a reflection of the correlation of K_{sym}, J and K_{NM} with L shown in Figure 8.

Figure 9 shows the correlation of the ISGMR centroid energies with W_0, the strength of the spin-orbit interaction. There is a positive strong correlation between the ^{48}Ca - ^{40}Ca energy difference and W_0. Similar results were obtained for the ISGDR, ISGQR and the ISGOR.

ISGDR

In Figure 10 the results of the self-consistent HF-based RPA calculations (full circles) for the ISGDR centroid energies of ^{40}Ca (a), ^{48}Ca (b), and the ^{48}Ca – ^{40}Ca energy difference (c), are compared with the experimental data [19,21]. The experimental values of E_{CEN} = 23.36 +/- 0.70 MeV for ^{40}Ca, E_{CEN} = 27.30 +/- 0.15 MeV for ^{48}Ca and their difference are shown in Figure 10 as the regions between the dashed lines. The HF-RPA energies, obtained for the interactions of Table 1, are plotted as a function of K_{NM}. For all the Skyrme interactions of Table 1, the calculated ISGDR centroid energies are higher than the experimental values by 1.5 – 6 MeV and the calculated ^{48}Ca - ^{40}Ca energy

difference, although positive, are smaller than the experimental value. We note that the experimental results for the fraction of the EWSR for the ISGDR in ^{48}Ca and ^{40}Ca are 137 +/- 20% and 62 +/- 20% [19,21], respectively, compared to the calculated values of 100%. Therefore, the comparison between the ISGDR in ^{48}Ca and ^{40}Ca might be misleading since only 62 +/- 20% of the EWSR of the ISGDR in ^{40}Ca was found experimentally. A strong correlation is also found between the ISGDR energy of ^{40}Ca with both K_{NM} and m*/m and similarly for ^{48}Ca.

ISGQR

Figure 11 shows, as a function of m*/m, our HF based RPA results (full circles) of the ISGQR centroid energies E_{CEN}, of ^{40}Ca (a), ^{48}Ca (b), and the ^{48}Ca - ^{40}Ca energy difference (c), obtained using the Skyrme type interactions of Table 1. The experimental values of E_{CEN} = 17.84 +/- 0.43 MeV for ^{40}Ca [19], E_{CEN} = 18.61 +/- 0.24 MeV for ^{48}Ca [21] and their difference are shown in Figure 11 as the regions between the dashed lines. As seen in Figure 11, a very strong correlation exists between the ISGQR energy of ^{40}Ca with m*/m and similarly for ^{48}Ca. We find that interactions having m*/m = 0.65 – 0.8 reproducing the experimental data of the ISGQR.

ISGOR

Figure 12 shows our HF based RPA results (full circles) of the ISGOR centroid energies E_{CEN}, of ^{40}Ca (a), ^{48}Ca (b), and the ^{48}Ca - ^{40}Ca energy difference (c), using the Skyrme type interactions of Table 1. A very strong correlation exists between the ISGOR of ^{40}Ca and ^{48}Ca with m*/m as can be seen in Figure 12. Using the result that interactions having m*/m = 0.65 – 0.8 reproduce the experimental data of the ISGQR we can predict the values of the E_{CEN} of the ISGOR in ^{40}Ca and ^{48}Ca to be in the region of 30 – 34 MeV.

For completeness we present in Table 4 the values of the Pearson correlations coefficients among the various NM properties and spin-orbit strength W_0 with the centroid energies of the isoscalar (T0) giant resonances of multipolarities *L= 0 – 3.* We find no correlations or very weak correlations between the ^{48}Ca – ^{40}Ca centroid energy differences of the isoscalar giant resonances with the coefficients J, L, or K_{sym}, associated with the density dependence of the symmetry energy and a strong correlation with the value of W_0.

IVGMR

For the IVGMR, an isovector compression mode, we show the HF-RPA results (full circles), obtained using for the Skyrme interactions of Table 1, for the centroid energies E_{CEN} of ^{40}Ca (a), ^{48}Ca (b) and the ^{48}Ca - ^{40}Ca energy difference (c) as a function of K_{NM} in Figure 13 and as a function of J in Figure 14. The experimental value of E_{CEN} = 31 +/- 2 MeV for ^{40}Ca [10,46] is shown as the region between the dashed lines. We find a medium correlation between E_{CEN} of the IVGMR with K_{NM} and a weak correlation with J, L or $K_{sym.}$ It can be seen from Figure 14 that a stronger correlation between the IVGMR energy and K_{NM} is obtained for a fixed value of J (at 27 and 30 MeV).

Figure 15 shows the IVGMR centroid energies as a function of W_0, the strength of the spin-orbit interaction. A strong positive correlation between the ^{48}Ca - ^{40}Ca energy difference and the value of W_0 is seen. Similar results were obtained for the IVGDR, and the IVGQR.

IVGDR

Figure 16 shows, as a function of J, our HF based RPA results (full circles) of the IVGDR centroid energies E_{CEN} of ^{40}Ca (a), ^{48}Ca (b), and the ^{48}Ca - ^{40}Ca energy difference

(c), obtained using the Skyrme type interactions of Table 1. The experimental values of E_{CEN} = 19.8 +/- 0.5 MeV for ^{40}Ca, E_{CEN} = 19.5 +/- 0.5 MeV for ^{48}Ca [48,49,50] and their difference are shown in Figure 16 as the regions between the dashed lines. Weak correlations can be seen between E_{CEN} of ^{40}Ca and E_{CEN} of ^{48}Ca with J. Similar results were obtained for L and K_{sym}.

Figure 17 shows the IVGDR centroid energies as a function of κ, the enhancement factor in the EWSR of the IVGDR. Strong positive correlations between the IVGDR centroid energy of ^{40}Ca and of ^{48}Ca with κ is seen in the Figure.

IVGQR

Figure 18 shows, as a function of m*/m, the HF based RPA results (full circles) of the IVGQR centroid energies E_{CEN} of ^{40}Ca (a), ^{48}Ca (b) and the ^{48}Ca - ^{40}Ca energy difference (c), obtained using the Skyrme type interactions of Table 1. The experimental data of E_{CEN} = 31 +/- 1.5 MeV for ^{40}Ca [51] is shown as the region between the dashed lines. Medium correlations between m*/m and E_{CEN} of ^{40}Ca and E_{CEN} of ^{48}Ca can be seen in Figure 18.

IVGOR

Figure 19 shows, as a function of m*/m, the HF based RPA results (full circles) of the IVGOR centroid energies E_{CEN} of ^{40}Ca (a), ^{48}Ca (b) and the ^{48}Ca - ^{40}Ca energy difference (c), obtained using the Skyrme type interactions of Table 1. Medium correlations between m*/m and E_{CEN} of ^{40}Ca and E_{CEN} of ^{48}Ca can be seen in Figure 19.

For completeness we present in Table 5 the values of the Pearson correlation coefficients among the various NM properties and spin-orbit strength W_0 with the centroid energies of the isovector (T1) giant resonances of multipolarities $L = 0 - 3$.

As shown in Table 5, only weak correlations exist between the E_{CEN} of the isovector giant resonances of ^{40}Ca or ^{48}Ca with J, L and K_{sym}. A strong correlation is found between the ^{48}Ca - ^{40}Ca centroid energy difference of the IVGMRs, IVDGRs, and IVGQRs with W_0. We also note the strong correlation between the E_{CEN} of the IVGDR and the value of κ.

4. Conclusions

We have presented results of our fully self-consistent HF-RPA calculations using 18 commonly employed Skyrme type interactions of Table 1, for the centroid energies of isoscalar and isovector giant resonances of multipolarities $L = 0 - 3$ in ^{40}Ca and ^{48}Ca and compared with available experimental data. We have investigated and discussed the sensitivity of the E_{CEN} of the giant resonances to various properties of NM. In particular we point out that:

- For all the 18 Skyrme interactions used in our HF-based RPA calculations (Table 1) the ^{48}Ca – ^{40}Ca centroid energy differences of the ISGMR are smaller than the experimental data. For 17 of the Skyrme interactions used in our HF-based RPA calculations the ^{40}Ca ISGMR lies above that for ^{48}Ca. The 18th interaction (SkI3) predicts the ISGMR in about the same location in both nuclei.
- We have demonstrated the very strong to strong correlations of the E_{CEN} of the compression modes, the ISGMR and the ISGDR, with the NM incompressibility coefficient K_{NM} and noted that the sensitivity of E_{CEN} to the effective mass is a reflection of the correlation between m*/m and K_{NM}, existing in the Skyrme interactions used in our calculations.

- For all the adopted Skyrme interactions, the calculated centroid energies of the ISGDR in ^{40}Ca and ^{48}Ca are consistently higher than the experimental data (by about 1.5 – 6 MeV).
- We have demonstrated the very strong correlation of E_{CEN} of the ISGQR and the ISGOR with m*/m. We have found that an agreement with the experimental data for E_{CEN} of the ISGQR in ^{40}Ca and ^{48}Ca is obtained for a value of the effective mass in the range of m*/m = 0.65 – 0.8. Using this result we can predict that the values of the E_{CEN} of the ISGOR in ^{40}Ca and ^{48}Ca should be in the region of 30 – 34 MeV.
- We find no correlations or very weak correlations between the ^{48}Ca – ^{40}Ca centroid energy differences of the isoscalar giant resonances of multipolariies L = 0 -3 with the coefficients J, L, or K_{sym}, associated with the density dependence of the symmetry energy. Similar results were found for the isovector giant resonances of multipolarities L = 0 – 3.
- We find positive strong correlations between the ^{48}Ca – ^{40}Ca centroid energy differences (ΔE_{CEN}) of the isoscalar and isovector giant resonances with W_0.
- For the IVGMR, the isovector compression mode, we find a medium correlation with K_{NM} and a weak correlation with J, L or $K_{sym.}$
- We find a weak correlation between the energies of the IVGDR of ^{40}Ca (and ^{48}Ca) and the quantities associated with the density dependence of the symmetry energy.
- We find a strong correlation between the energies of the IVGDR of ^{40}Ca (and ^{48}Ca) and the value of κ.
- For the IVGQR and IVGOR we find a strong correlation between E_{CEN} and m*/m.

The disagreement between the HF-RPA results and the experimental data for the centroid energies of the ISGMR and ISGDR in ^{40}Ca and ^{48}Ca remain unsolved problems which call for possible extension of the EDF used in the work, microscopic calculations of the excitation cross sections of giant resonances [38,52] and/or going beyond the HF-RPA theory [53].

Acknowledgements

This work was supported in part by US Department of Energy under Grant No. DOE-FG03-93ER40773.

References

[1] A. Bohr and B. M. Mottelson, *Nuclear Structure II, (Benjamin, New York, 1975).*

[2] P. Ring and P. Schuck, *The nuclear many-body problem*, (Springer, New York -Heidelberg-Berlin, 1980).

[3] S. Shlomo, V. M. Kolomietz, and G. Colo, Eur. Phys. J. **A30**, 23 (2006) and references therein.

[4] N. K. Glendening, Phys. Rev. C **37**, 2733 (1988).

[5] J. M. Lattimer and M. Prakash, Phys. Rep. **442**, 109 (2007).

[6] W. D. Myers and W. J. Swiatecki, Phys. Rev. C **57**, 3020 (1998).

[7] L. Satpathy, V. S. U. Maheshwari and R. C. Nayak, Phys. Rep. **319**, 85 (1999).

[8] J.P. Blaizot, Phys. Rep. **64**, 171 (1980).

[9] H. Krivine, J. Treiner and O. Bohigas, Nucl. Phys. **A336**, 155 (1984).

[10] E. Lipparini and S. Stringari, Phys. Rep. **175**, 103 (1989).

[11] J. Treiner, H. Krivine, and O. Bohigas, Nucl. Phys. **A371**, 253 (1981).

[12] D. H. Youngblood, P. Bogucki, J. D. Bronson, U. Garg, Y.-W. Lui, and C. M. Rozsa, Phys. Rev. C **23**, 1997 (1981).

[13] B. K. Jennings and A. D. Jackson, Phys. Rep. **66**, 141 (1980).

[14] S. Shlomo and D.H. Youngblood, Phys. Rev. C **47**, 529 (1993), and references therein.

[15] J. M. Pearson, N. Chamel and S. Goriely, Phys. Rev. C **82**, 037301 (2010).

[16] T.H.R. Skyrme, Phil. Mag. **1**, 1043 (1956).

[17] T.H.R. Skyrme, Nucl. Phys. **9**, 615 (1959).

[18] D. Vautherin and D. M. Brink, Phys. Rev. C **5**, 626 (1972).

[19] Y.-W. Lui, D.H. Youngblood, S. Shlomo, X. Chen, Y. Tokimoto, Krishichayan, M. Anders, and J. Button, Phys. Rev. C. **83**, 044327 (2011).

[20] D.H. Youngblood, Y.-W. Lui, H.L. Clark, Y. Tokimoto, and B. John, Phys. Rev. C **68**, 057303 (2003).

[21] D.H. Youngblood, Y.-W. Lui, and H.L. Clark, Phys. Rev. C **63**, 067301 (2001).

[22] D.H. Youngblood, Y.-W. Lui, and H.L. Clark, Phys. Rev. C **55**, 2811 (1997).

[23] Nguyen Van Giai and H. Sagawa, Phys. Lett. **106B**, 379 (1981).

[24] B.K. Argawal, S. Shlomo, and V. Kim Au, Phys. Rev. C **72**, 014310 (2005).

[25] J. Bartel, P. Quentin, M. Brack, C. Guet, and H.B. Hakansson, Nucl. Phys. **A382**, 79 (1986).

[26] B.K. Argawal, S. Shlomo, and V. Kim Au, Phys. Rev. C **68**, 031304 (2003).

[27] S. Shlomo and G. Bertsch, Nucl. Phys. **A243**, 507 (1975).

[28] P. -G. Reinhardt, Ann. Phys. (Leipzig) **1**, 632 (1992).

[29] T. Nakatsukasa, T. Inakura and K. Yabana, Phys. Rev. C **76**, 024318 (2007).

[30] E. Chabanat, P. Bonche, P. Haensel, J. Meyer and R. Schaeffer, Nucl. Phys. **A627**, 710 (1997).

[31] W. Kohn, Rev. Mod. Phys. **71**, 1253 (1999).

[32] S. Shlomo, Rep. Prog. Phys. **41**, 957 (1978).

[33] M. Bender, P. H. Heenen, and P.-G. Reinhard, Rev. Mod. Phys. **75**, 121 (2003).

[34] M. Dutta, O. Lourenco, J. S. Sa Martins, A.Delfino, J. R. Stone and P. D. Stevenson, ArXiv:1202.3902v1, Phys. Rev. C.**85**, 035201 (2012).

[35] S. Shlomo and W. G. Love, Physica Scripta **26**, 280 (1982).

[36] Tapas Sil, S. Shlomo, B.K. Agrawal, and P.-G. Reinhard, Phys. Rev. C **73**, 034316 (2006).

[37] V. O. Nesterenko1, J. Kvasil2, and P.-G. Reinhard, Phys. Rev. C **66**, 044307 (2002).

[38] S. Shlomo and A. I. Sanzhur, Phys. Rev. C **65**, 044310 (2003).

[39] B. K. Agrawal, S. Shlomo and A. I. Sanzhur, Phys. Rev. C **67**, 034314 (2003).

[40] P. -G. Reinhard, and H. Flocard, Nucl. Phys. **A587**, 467 [1995].

[41] P. Klupfel, P. -G. Reinhard, T. J. Burvenich and J. A. Maruhn, Phys. Rev. C **79,** 034310 (2009).

[42] N. Lyutorovich, V. I. Tselyaev, J. Speth, S. Krewalsd, F. Grummer and P.-G. Reinhard, Phys. Rev. Lett. **109**, 092502 (2012).

[43] E. Chabanat, P. Bonche, P. Haensel, J. Meyer and R. Schaeffer, Nucl. Phys. **A635**, 231 (1998).

[44] L. Bennour, P.-H. Heenen, P. Bonche, J. Dobaczewski and H. Flocard, Phys. Rev. C **40**, 2834 (1989).

[45] J. Dobaczewski, H. Flocard, and J. Treiner. Nucl. Phys. **A422**, 103-139 (1984).

[46] P.-G Reinhard, D. J. Dean, W. Nazarewicz, J. Dobaczewski, J. A. Maruhn, and M. R. Strayer, Phys. Rev. C **60**, 014316 (1999).

[47] E. Erell, J. Alster, J. Lichtenstadt, M. A. Moinester, J. D. Bowman, M. D. Cooper, F. Irom, H. S. Matis, E. Piasetzky, and U. Sennhauser, Phys. Rev. C **34**, 1822 (1986).

[48] P. Gleissl, M. Brack, J. Meyer, and P. Quentin, Ann. of Phys. **197,** 205 (1990).

[49] A. Veyssière, H. Beil, R. Bergère, P. Carlos, A. Leprêtre, and A. De Miniac, Nucl. Phys. **A277**, 513 (1974).

[50] G. J. O'keefe, M. N. Thompson, Y. I. Assafiri, R. E. Pywell and K. Shoda, Nucl. Phys. **A469**, 239 (1987).

[51] D. A. Sims *et al*., Phys. Rev. C **55**, 1288 (1997).

[52] A. Kolomiets, O. Pochivalov and S. Shlomo, Phys. Rev. C **61**, 034312-1-8 (2000).

[53] S. Kamerdzhiev, J. Speth, and G. Tertchny, Eur. Phys. J. A **7**, 483 (2000); S. Kamerdzhiev, J. Speth, and G. Tertchny, Phys. Reports **393**, 1 (2004).

FIGURE CAPTIONS

Fig. 1. (Color online) Self-consistent HF-based RPA results (solid lines) for the distribution of the energy-weighted strength, normalized to one (fraction of EWSR), for the isoscalar monopole (E0), dipole (E1), quadrupole (E2), and octopole (E3) in ^{40}Ca, obtained using the KDE0 [24] Skyrme interaction. For the purpose of comparison with

experiment a Lorenzian smearing of a 3 MeV width was used in the calculation. The experimental data [21] are shown as histograms.

Fig. 2. (Color online) Same as Fig. 1 except for ^{48}Ca. Experimental data is from Ref. [19].

Fig. 3. (Color online) Self-consistent HF-based RPA results (solid lines) for the distribution of the energy-weighted strength, normalized to one (fraction of EWSR), for the isovector monopole (E0), dipole (E1), quadrupole (E2), and octopole (E3) in ^{40}Ca, obtained using the KDE0 [24] Skyrme interaction. A Lorenzian smearing of a 3 MeV width was used in the calculation.

Fig. 4. (Color online) Same as Fig. 3 except for ^{48}Ca.

Fig. 5. Comparison of experimental data [19,21] of the ISGMR centroid energies of ^{40}Ca (a), ^{48}Ca (b) and the ^{48}Ca – ^{40}Ca energy difference (c), shown as the regions between the dashed lines, with the results of fully self-consistent HF based RPA calculations (full circles) obtained using the Skyrme interactions of Table 1, plotted vis. K_{NM}. The results obtained with violation of self-consistency in the RPA calculations, are shown in (d).

Fig. 6. The values of ρ_0, m*/m, and J are plotted vs. $K_{NM,}$ for the Skyrme interactions of Table 1.

Fig 7. The HF based RPA results (full circles) of the ISGMR centroid energies E_{CEN} of ^{40}Ca (a), ^{48}Ca (b) and the ^{48}Ca – ^{40}Ca energy difference (c), obtained using the Skyrme type interactions of Table 1, as a function of the NM symmetry energy at saturation density J. The limits on the experimental data are shown by the dashed lines.

Fig. 8. The values of K_{sym}, J, and K_{NM} are plotted vs. L, for the Skyrme interactions of Table 1.

Fig. 9. Same as Fig. 7 except as a function of the strength W_0 of the spin-orbit interaction.

Fig. 10. Same as Fig. 7 except for the ISGDR as a function of $K_{NM.}$

Fig. 11. Same as Fig. 7 except for the ISGQR as a function of m*/m.

Fig. 12. Same as Fig. 11 except for the ISGOR.

Fig. 13. Same as Fig. 7 except for the IVGMR as a function of $K_{NM.}$ The experimental data is taken from Ref. [10,47]

Fig. 14. Same as Fig. 13 except as a function of J.

Fig. 15. Same as Fig. 13 except as a function of W_0.

Fig. 16. Same as Fig. 7 except for the IVGDR. The experimental data is taken from Ref. [48,49,50].

Fig. 17. Same as Fig. 16 except as a function of κ.

Fig. 18. Same as Fig. 11 except for the IVGQR. The experimental data is taken from Ref. [51].

Fig. 19. Same as Fig. 18 except for the IVGOR.

Table 1. Values for the parameters for the following Skyrme interactions: SGII [23], KDE0 [24], KDE0v1 [24], SKM* [25], SK255 [26], SkI3 [40], SkI4 [40], SkI5 [40], SV-bas [41], SV-min [41], SV-m56-O [42], SV-m64-O [42], SLy6 [43], SLy4 [43], SLy5 [43], SkMP [44], SkP [45] and SkO' [46]. These parameters are given in the following units: t_0 [MeV fm^3], t_1 [MeV fm^5], t_2 [MeV fm^5], t_3 [MeV fm$^{3(\alpha+1)}$], W_0 [MeV], and the remaining parameters are dimensionless.

Force	t_0	t_1	t_2	t_3	W_0	x_0	x_1	x_2	x_3	X_w	α
SGII	-2645.00	340.00	-41.90	15595.00	105.00	0.0900	-0.0588	1.4250	0.0604	1.0000	1/6
KDE0	-2526.51	430.94	-398.38	14235.52	128.96	0.7583	-0.3087	-0.9495	1.1445	1.0000	0.1676
KDE0v1	-2553.08	411.70	-419.87	14603.61	124.41	0.6483	-0.3472	-0.9268	0.9475	1.0000	0.1673
SKM*	-2645.00	410.00	-135.00	15595.00	130.00	0.0900	0.0000	0.0000	0.0000	1.0000	1/6
SK255	-1689.35	389.30	-126.07	10989.60	95.39	-0.1461	0.1660	0.0012	-0.7449	1.0000	0.3563
SkI3	-1762.88	561.61	-227.09	8106.20	188.51	0.3083	-1.1722	-1.0907	1.2926	0.0000	1/4
SkI4	-1885.83	473.83	1006.86	9703.61	366.19	0.4051	-2.8891	-1.3252	1.1452	-0.9850	1/4
SkI5	-1772.91	550.84	-126.69	8206.25	123.63	-0.1171	-1.3088	-1.0487	0.3410	1.0000	1/4
SV-bas	-1879.64	313.75	112.68	12527.38	124.63	0.2585	-0.3817	-2.8236	0.1232	0.5474	0.3000
SV-min	-2112.25	295.78	142.27	13988.57	111.29	0.2439	-1.4349	-2.6259	0.2581	0.8255	0.2554
SV-m56-O	-1905.40	571.19	1594.80	8439.04	133.27	0.6440	-2.9737	-1.2553	1.7966	0.7949	0.2000
SV-m64-O	-2083.86	484.60	1134.35	10720.67	113.97	0.6198	-2.3327	-1.3059	1.2101	1.1042	0.2000
SLy4	-2488.91	486.82	-546.39	13777.00	123.00	0.8340	-0.3440	-1.0000	1.3540	1.0000	1/6
SLy5	-2484.88	483.13	-549.40	13763.00	126.00	0.7780	-0.3280	-1.0000	1.2670	1.0000	1/6
SLy6	-2479.50	462.18	-448.61	13673.00	122.00	0.8250	-0.4650	-1.0000	1.3550	1.0000	1/6
SkMP	-2372.24	503.62	57.28	12585.30	160.00	-0.1576	-0.4029	-2.9557	-0.2679	1.0000	1/6
SkP	-2931.70	320.62	-337.41	18708.97	100.00	0.2922	0.6532	-0.5373	0.1810	1.0000	1/6
SkO'	-2099.42	301.53	154.78	13526.46	287.79	-0.0295	-1.3257	-2.3234	-0.1474	-0.5760	1/4

Table 2. Same as Table 1 with the following conditions defining the interactions: HBTM, for proton and neutron $\hbar^2/2m$ = 20.7525 MeV fm^2 for 0, for proton $\hbar^2/2m$ = 20.7213 MeV fm^2 and neutron $\hbar^2/2m$ = 20.7498 MeV fm^2 for 1, and for proton and neutron $\hbar^2/2m$ = 20.7355 MeV fm^2 for 2, JTM, contribution to the spin-orbit potential from t_1 and t_2 is taken for 1 and not for 0, CEX, coulomb-exchange on for 1 and off for 0, RHOC, proton-density is used for coulomb potential for 0 and charge-density is used for coulomb potential for 1, and ZPE, center of mass correction is taken as (1-1/A) factor on the mass for 1 and is computed explicitly a posteriori as $E_{CM} = \frac{1}{2mA}\langle \hat{P}^2 \rangle$ for 0.

Force	Ref.	HBTM	JTM	CEX	RHOC	ZPE
SGII	[23]	0	0	1	0	0
KDE0	[24]	2	1	0	0	1
KDE0v1	[24]	2	1	0	0	1
SKM*	[25]	0	0	1	0	0
SK255	[26]	2	1	0	0	1
SkI3	[40]	0	0	1	0	1
SkI4	[40]	0	0	1	0	1
SkI5	[40]	0	0	1	0	1
SV-bas	[41]	1	0	1	0	1
SV-min	[41]	1	0	1	0	1
SV-m56-O	[42]	1	0	1	0	1
SV-m64-O	[42]	1	0	1	0	1
SLy4	[43]	2	0	1	0	0
SLy5	[43]	2	1	1	0	0
SLy6	[43]	2	0	1	0	1
SkMP	[44]	0	0	1	0	0
SkP	[45]	2	1	1	0	0
SkO'	[46]	2	1	1	0	1

Table 3. Properties of symmetric nuclear matter at nuclear saturation density ρ_0 [fm^3] associated with the Skyrme interactions of Table. Also shown are the total binding energy per nucleon E/A [MeV], isoscalar effective mass m*/m, incompressibility modulus K_{NM} [MeV], the coefficients related to the symmetry energy density J [MeV], L [MeV] and K_{sym} [MeV], and the enhancement factor of the EWSR of the IVGDR, κ.

	E/A	ρ_0	m*/m	K_{NM}	J	L	K_{sym}	κ
SGII	15.59	0.159	0.79	215.0	26.80	37.63	-145.90	0.49
KDE0	16.11	0.161	0.72	228.8	33.00	45.22	-144.78	0.30
KDE0v1	16.23	0.165	0.74	227.5	34.58	54.70	-127.12	0.23
SKM*	15.78	0.160	0.79	216.7	30.03	45.78	-155.94	0.53
SK255	16.33	0.157	0.80	255.0	37.40	95.00	-58.33	0.54
SkI3	15.96	0.158	0.58	258.1	34.80	100.52	73.04	0.25
SkI4	15.92	0.160	0.65	247.9	29.50	60.39	-40.56	0.25
SkI5	15.83	0.156	0.58	255.7	36.70	129.33	159.57	0.25
SV-bas	15.90	0.160	0.90	234.0	30.00	45.21	-221.75	0.40
SV-min	15.91	0.161	0.95	222.0	30.01	44.76	-156.57	0.08
SV-m56-O	15.81	0.157	0.56	254.6	27.00	49.96	-45.04	0.60
SV-m64-O	15.82	0.159	0.64	241.5	27.01	30.63	-144.76	0.60
SLy4	15.97	0.160	0.70	229.9	32.00	45.96	-119.73	0.25
SLy5	15.98	0.160	0.70	229.9	32.03	48.27	-112.76	0.25
SLy6	15.92	0.159	0.69	229.8	31.96	47.44	-112.71	0.25
SkMP	15.56	0.157	0.65	230.9	29.88	70.31	-49.82	0.71
SkP	15.93	0.162	1.00	200.8	32.98	45.21	-266.60	0.30
SkO'	15.75	0.160	0.90	222.3	31.95	68.93	-78.82	0.15

`

Table 4**.** Pearson correlation coefficients among the various NM properties and spin-orbit strength W_0 with the centroid energies of the isoscalar T0 giant resonances of multipolarities $L = 0 - 3$.

			m*/m	K_{NM}	J	L	K_{sym}	κ	$W_0 (X_W=1)$
L0 T0	Ca 40	E_{CEN}	-0.75	0.95	0.07	0.56	0.78	0.20	0.00
L0 T0	Ca 48	E_{CEN}	-0.79	0.88	0.02	0.56	0.80	0.24	0.30
L0 T0		ΔE_{CEN}	-0.31	0.07	-0.11	0.16	0.25	0.18	0.73
L1 T0	Ca 40	E_{CEN}	-0.84	0.74	-0.20	0.30	0.64	0.47	0.24
L1 T0	Ca 48	E_{CEN}	-0.89	0.71	-0.11	0.25	0.62	0.25	0.46
L1 T0		ΔE_{CEN}	-0.30	0.14	0.11	-0.02	0.12	-0.28	0.54
L2 T0	Ca 40	E_{CEN}	-0.97	0.81	-0.03	0.40	0.76	0.22	0.48
L2 T0	Ca 48	E_{CEN}	-0.97	0.75	-0.06	0.36	0.74	0.22	0.57
L2 T0		ΔE_{CEN}	-0.20	-0.26	-0.20	-0.18	-0.02	0.00	0.52
L3 T0	Ca 40	E_{CEN}	-0.96	0.80	-0.05	0.35	0.73	0.23	0.41
L3 T0	Ca 48	E_{CEN}	-0.98	0.73	-0.08	0.33	0.72	0.27	0.59
L3 T0		ΔE_{CEN}	-0.11	-0.25	-0.13	-0.07	-0.01	0.16	0.56

Table 5. Pearson correlation coefficients among the various NM properties and spin-orbit strength W_0 with the centroid energies of the isovector T1 giant resonances of multipolarities $L = 0 - 3$.

			m*/m	K_{NM}	J	L	K_{sym}	κ	$W_0 (X_W=1)$
L0 T1	Ca 40	E_{CEN}	-0.54	0.66	-0.33	0.10	0.31	0.61	0.01
L0 T1	Ca 48	E_{CEN}	-0.64	0.62	-0.35	0.17	0.40	0.74	0.36
L0 T1		ΔE_{CEN}	-0.25	-0.10	-0.06	0.16	0.22	0.31	0.70
L1 T1	Ca 40	E_{CEN}	-0.34	0.31	-0.58	-0.40	-0.17	0.66	-0.07
L1 T1	Ca 48	E_{CEN}	-0.36	0.28	-0.63	-0.40	-0.17	0.73	0.23
L1 T1		ΔE_{CEN}	-0.01	-0.22	-0.09	0.09	0.07	0.14	0.67
L2 T1	Ca 40	E_{CEN}	-0.64	0.52	-0.47	-0.14	0.16	0.68	0.43
L2 T1	Ca 48	E_{CEN}	-0.70	0.49	-0.50	-0.14	0.19	0.73	0.66
L2 T1		ΔE_{CEN}	-0.33	-0.10	-0.18	0.02	0.14	0.27	0.71
L3 T1	Ca 40	E_{CEN}	-0.73	0.61	-0.33	0.04	0.36	0.60	0.37
L3 T1	Ca 48	E_{CEN}	-0.71	0.56	-0.43	-0.07	0.26	0.65	0.42
L3 T1		ΔE_{CEN}	0.34	-0.42	-0.21	-0.41	-0.47	-0.08	-0.11

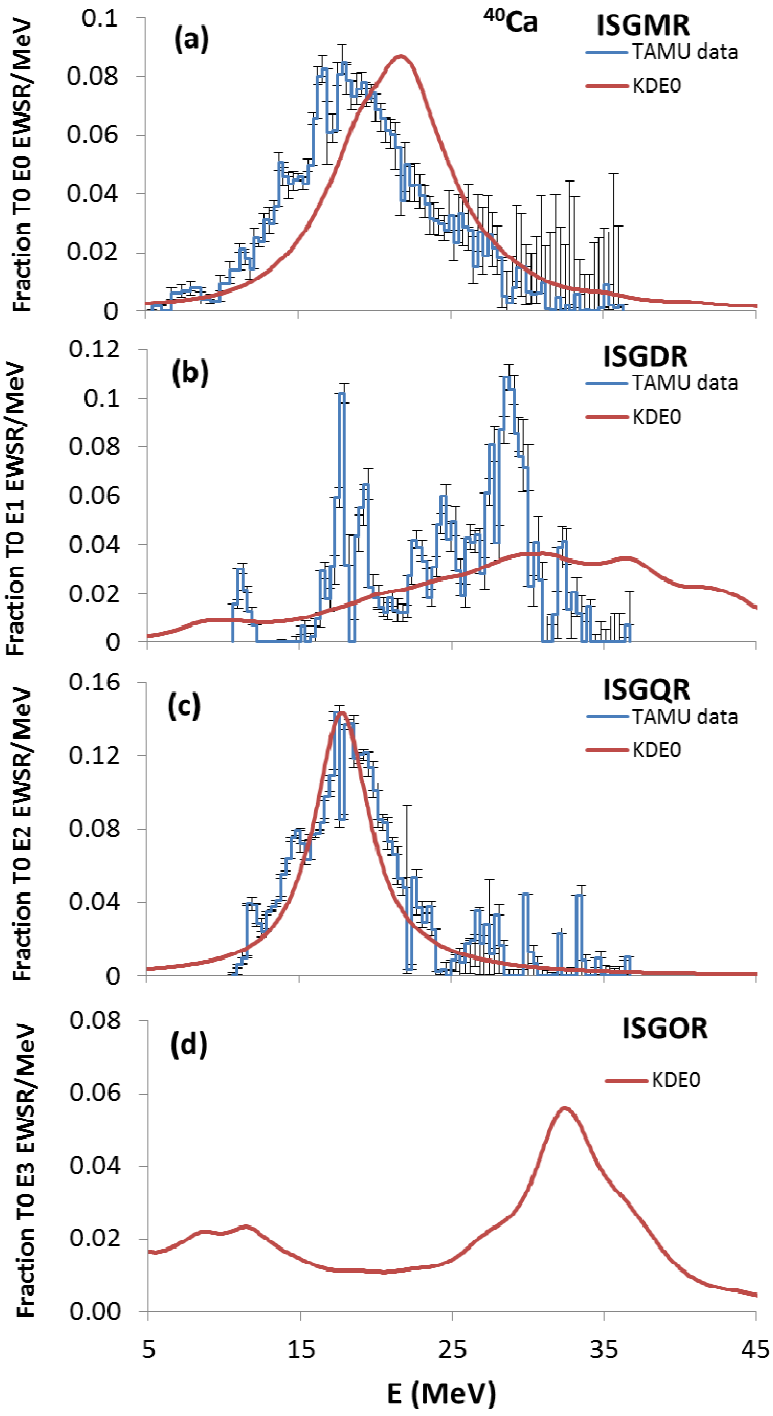

Fig. 1. (Color online) Self-consistent HF-based RPA results (solid lines) for the distribution of the energy-weighted strength normalized to one (fraction of EWSR) for the isoscalar monopole (E0), dipole (E1), quadrupole (E2), and octopole (E3) in ^{40}Ca, obtained using the KDE0 [24] Skyrme interaction. A Lorenzian smearing of a 3 MeV width was used in the calculation. The experimental data [21] are shown as histograms.

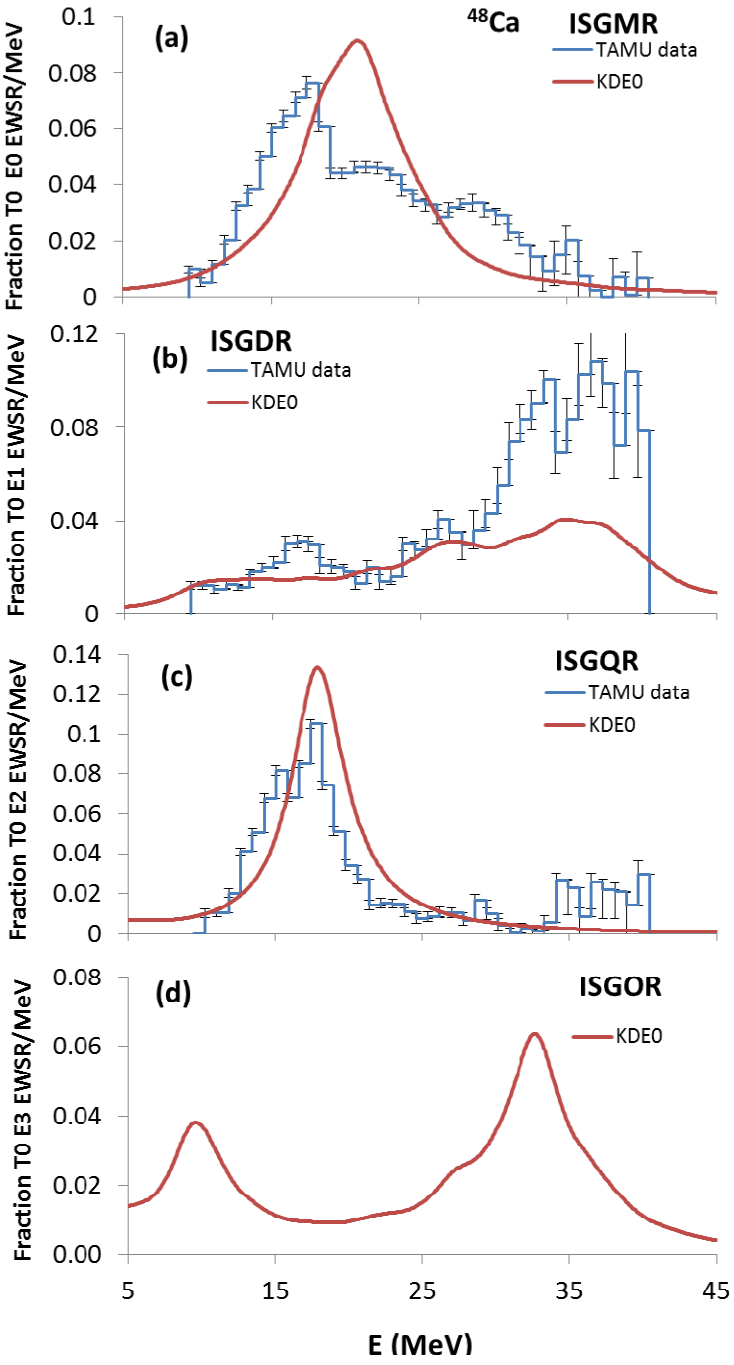

Fig. 2. (Color online) Same as Fig. 1 except for ^{48}Ca. Experimental data is from Ref. [19].

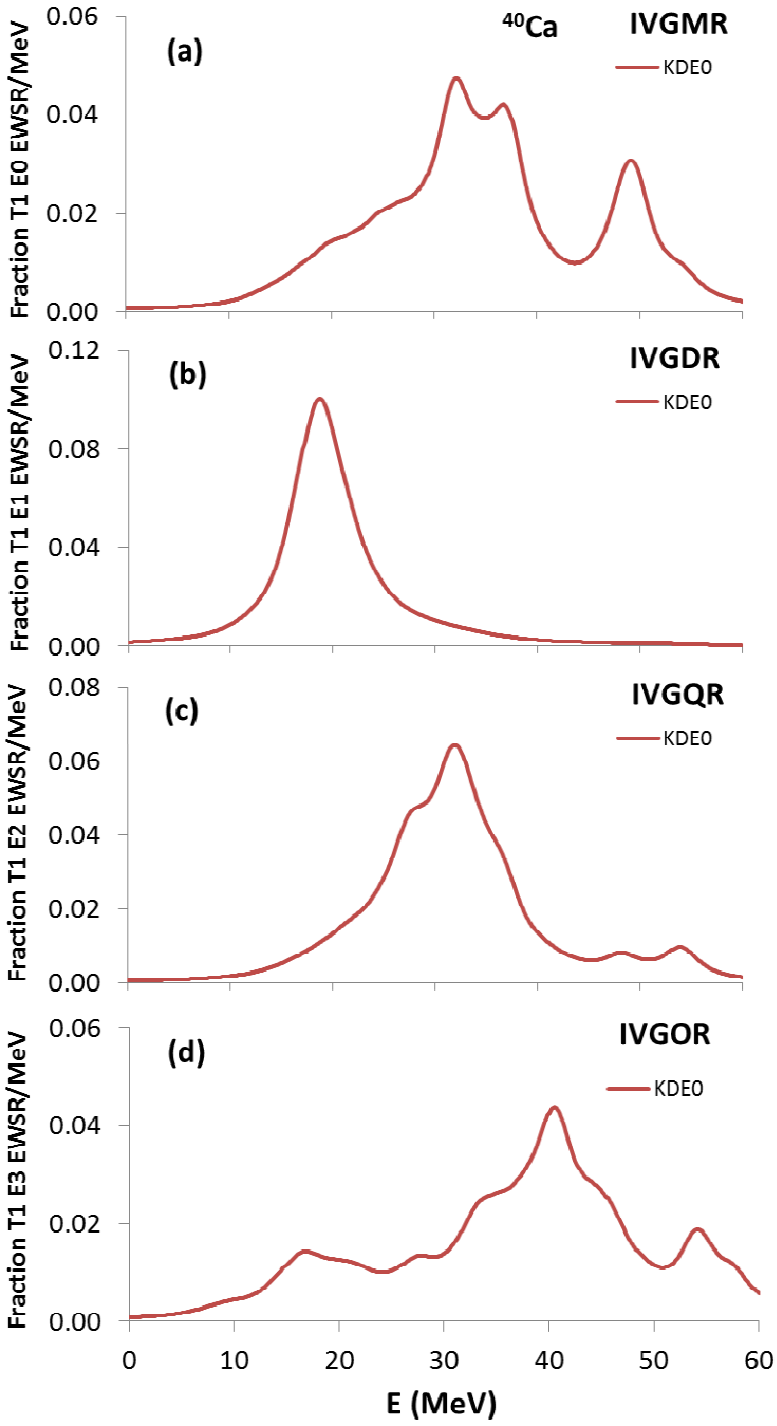

Fig. 3. (Color online) Self-consistent HF-based RPA results (solid lines) for the distribution of the energy-weighted strength, normalized to one (fraction of EWSR), for the isovector monopole (E0), dipole (E1), quadrupole (E2), and octopole (E3) in ^{40}Ca, obtained using the KDE0 [24] Skyrme interaction. A Lorenzian smearing of a 3 MeV width was used in the calculation.

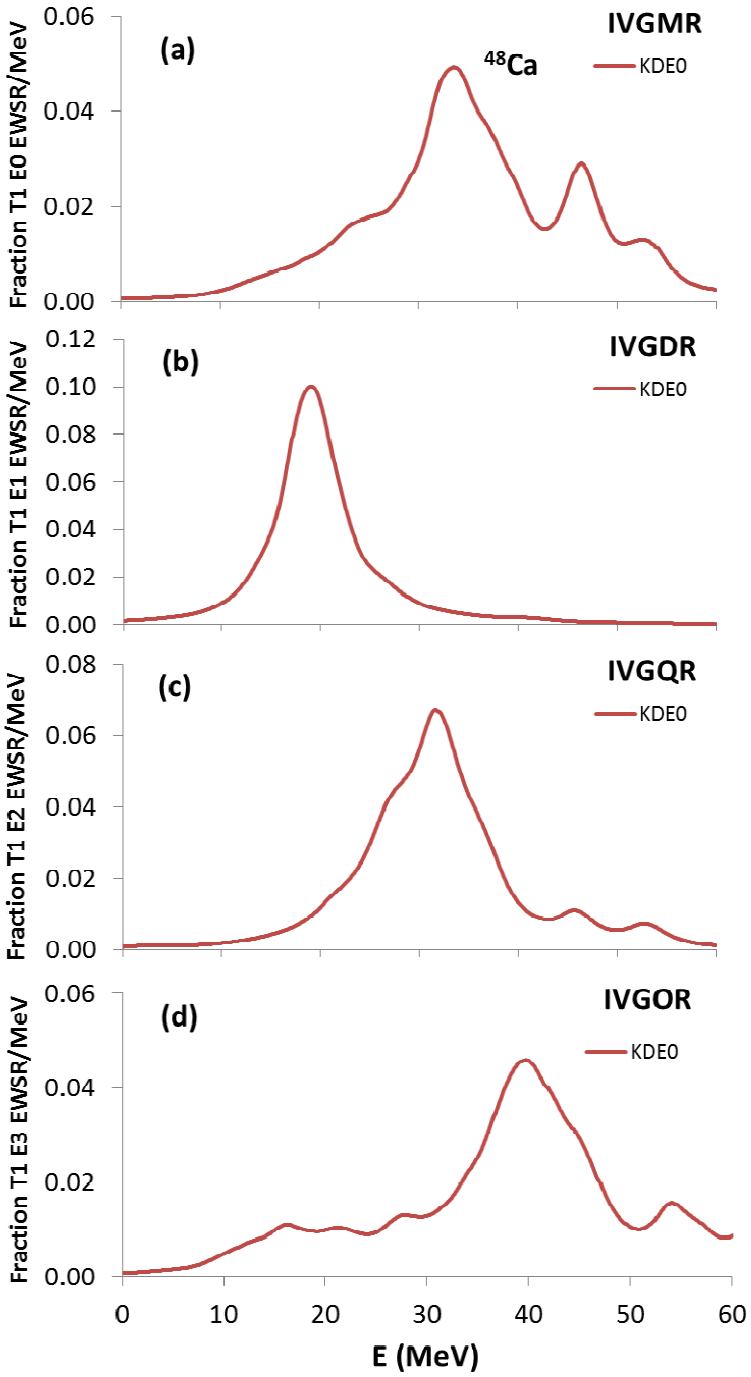

Fig. 4. (Color online) Same as Fig. 3 except for ^{48}Ca.

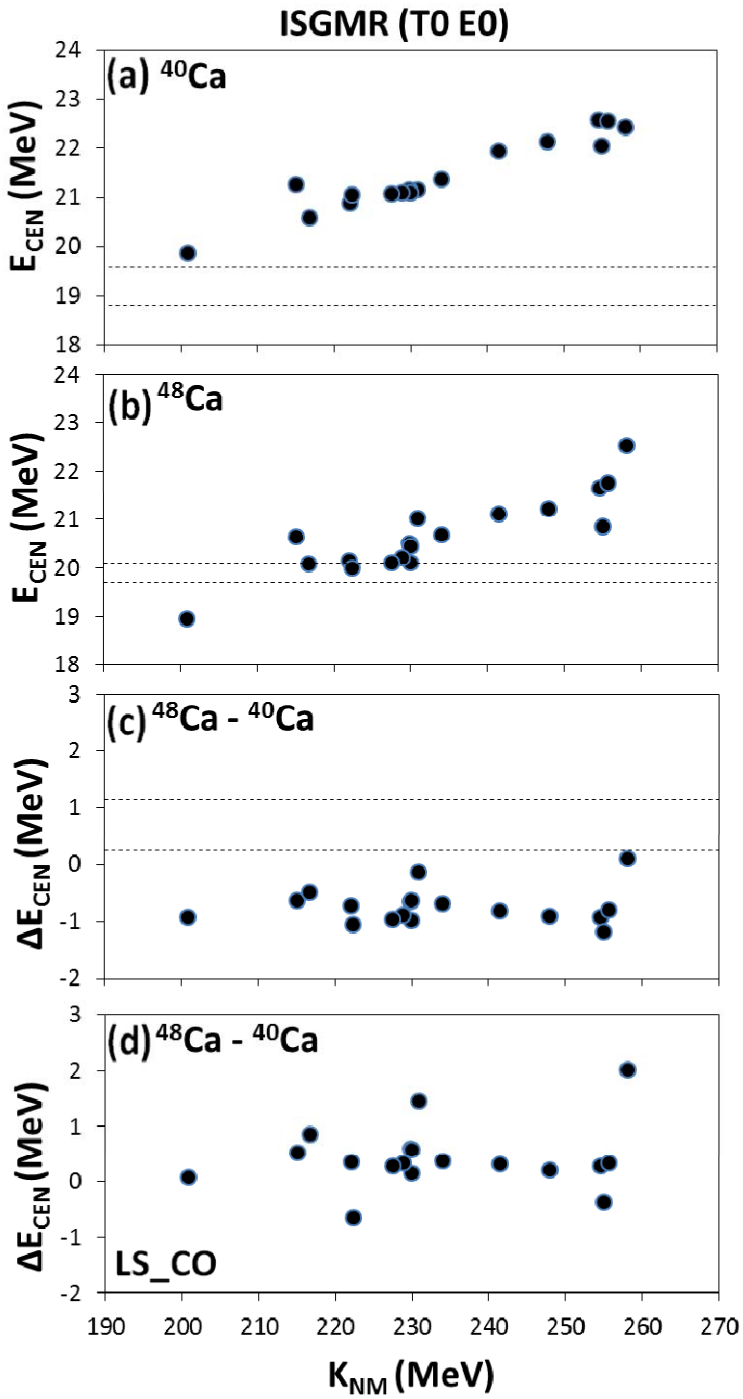

Fig. 5. Comparison of experimental data [19,21] of the ISGMR centroid energies of ^{40}Ca (a), ^{48}Ca (b), and the ^{48}Ca – ^{40}Ca energy difference (c), shown as the regions between the dashed lines, with the results of fully self-consistent HF based RPA calculations (full circles) obtained using the Skyrme interactions of Table 1, plotted vis. K_{NM}. The results obtained with violation of self-consistency in the RPA calculations, are shown in (d).

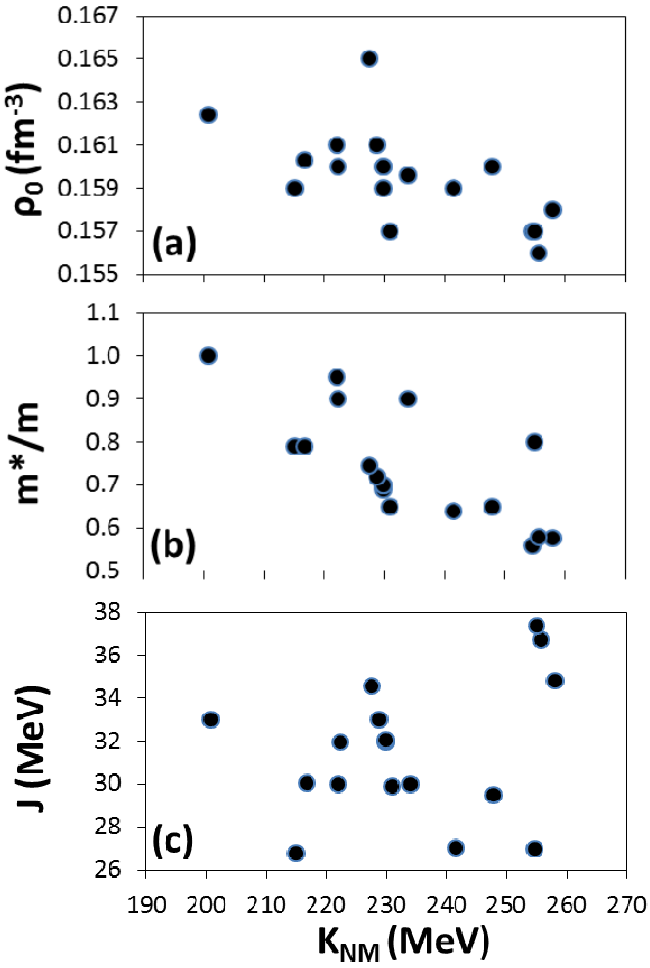

Fig. 6. The values of , m*/m, and J are plotted vs. $K_{NM,}$ for the Skyrme interactions of Table 1.

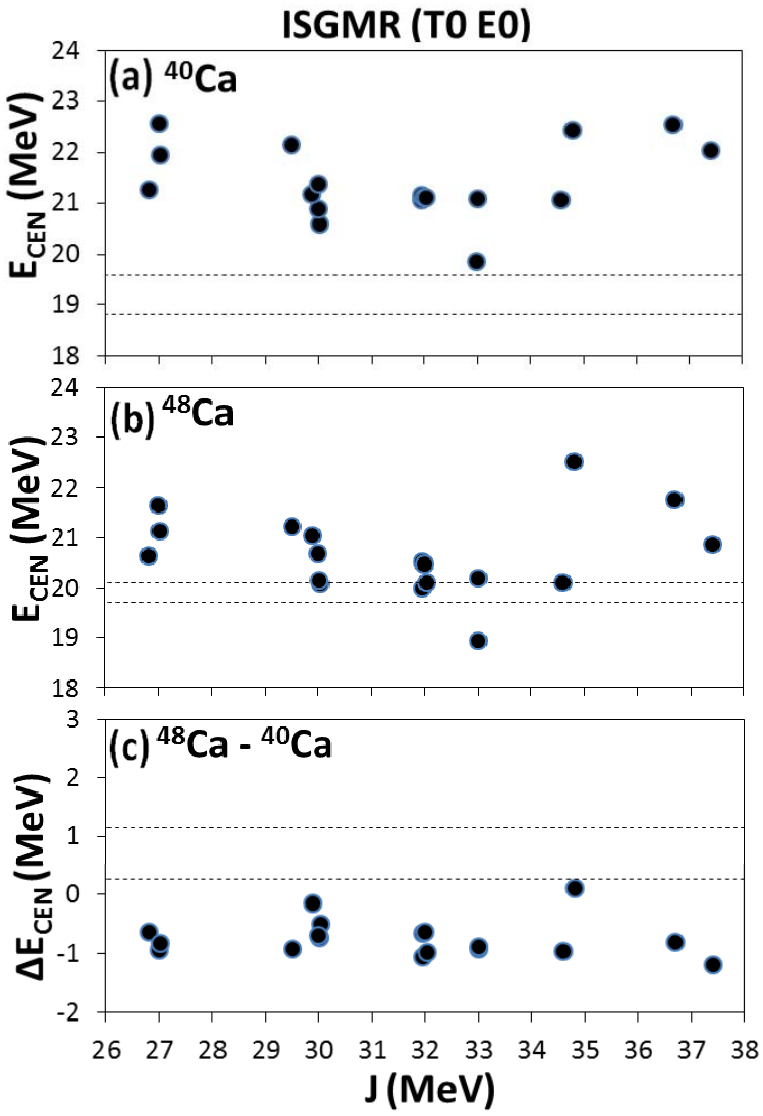

Fig 7. The HF based RPA results (full circles) of the ISGMR centroid energies E_{CEN} of ^{40}Ca (a), ^{48}Ca (b) and the ^{48}Ca – ^{40}Ca energy difference (c), obtained using the Skyrme type interactions of Table 1, as a function of the NM symmetry energy at saturation density J. The limits on the experimental data are shown by the dashed lines.

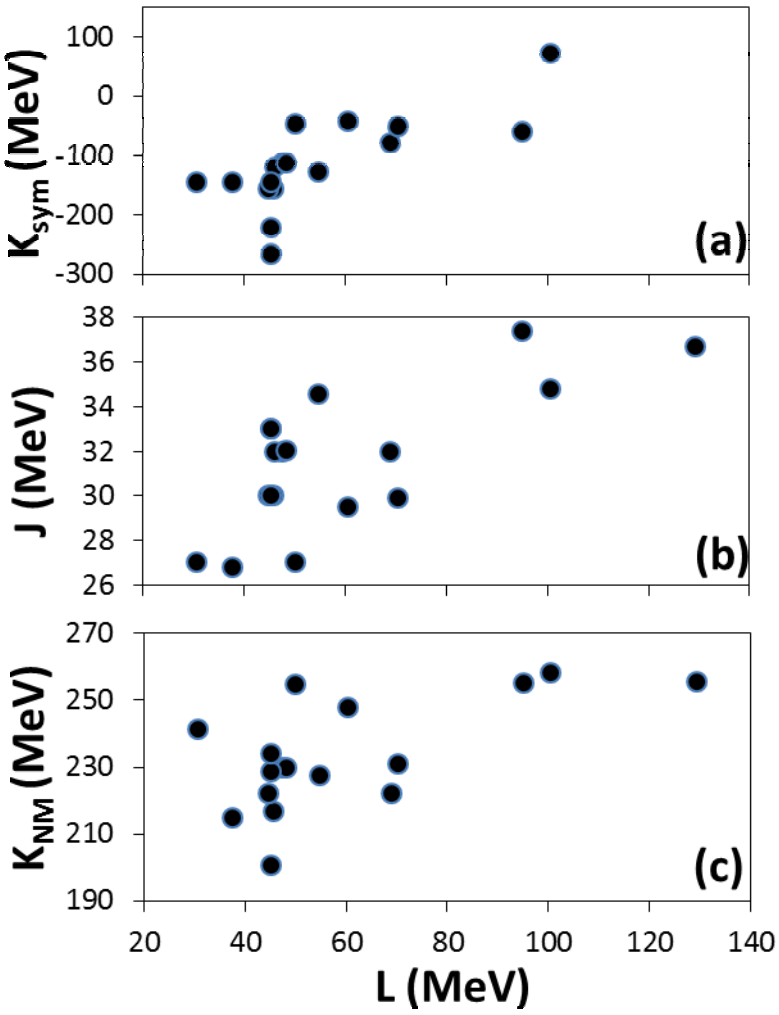

Fig. 8. The values of K_{sym}, J, and K_{NM} are plotted vs. L, for the Skyrme interactions of Table 1

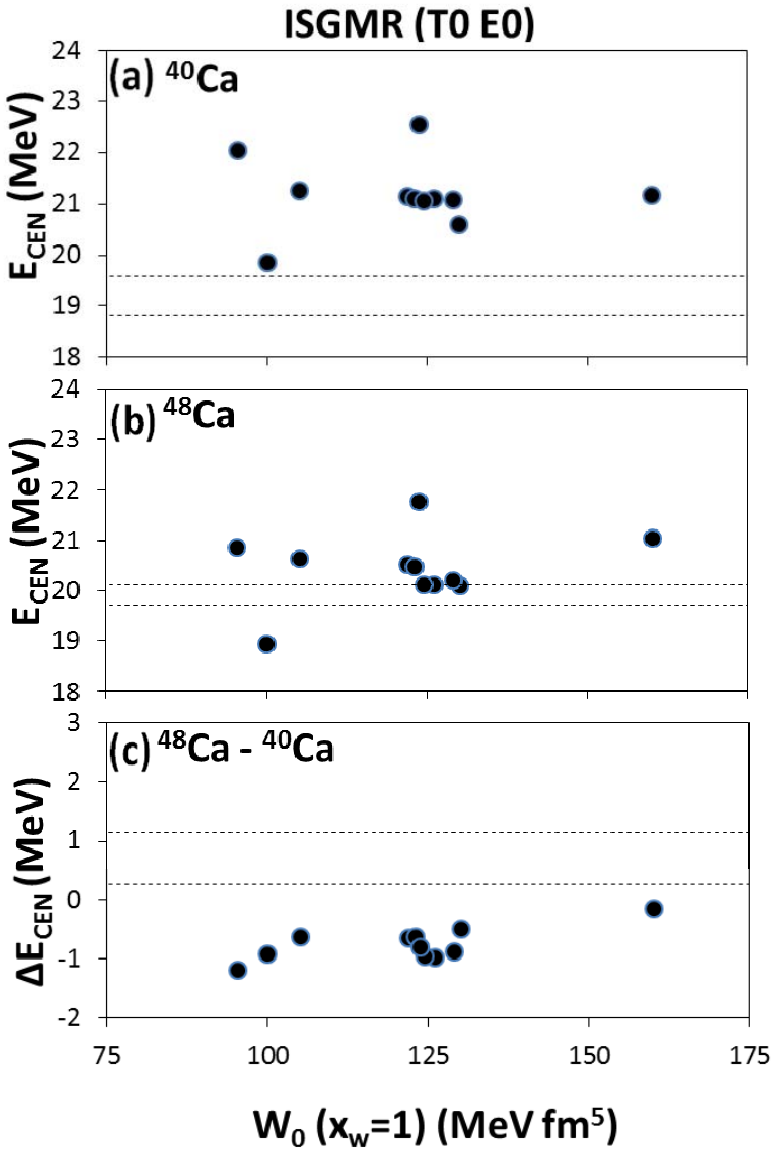

Fig. 9. Same as Fig. 7 except as a function of the strength W_0 of the spin-orbit interaction.

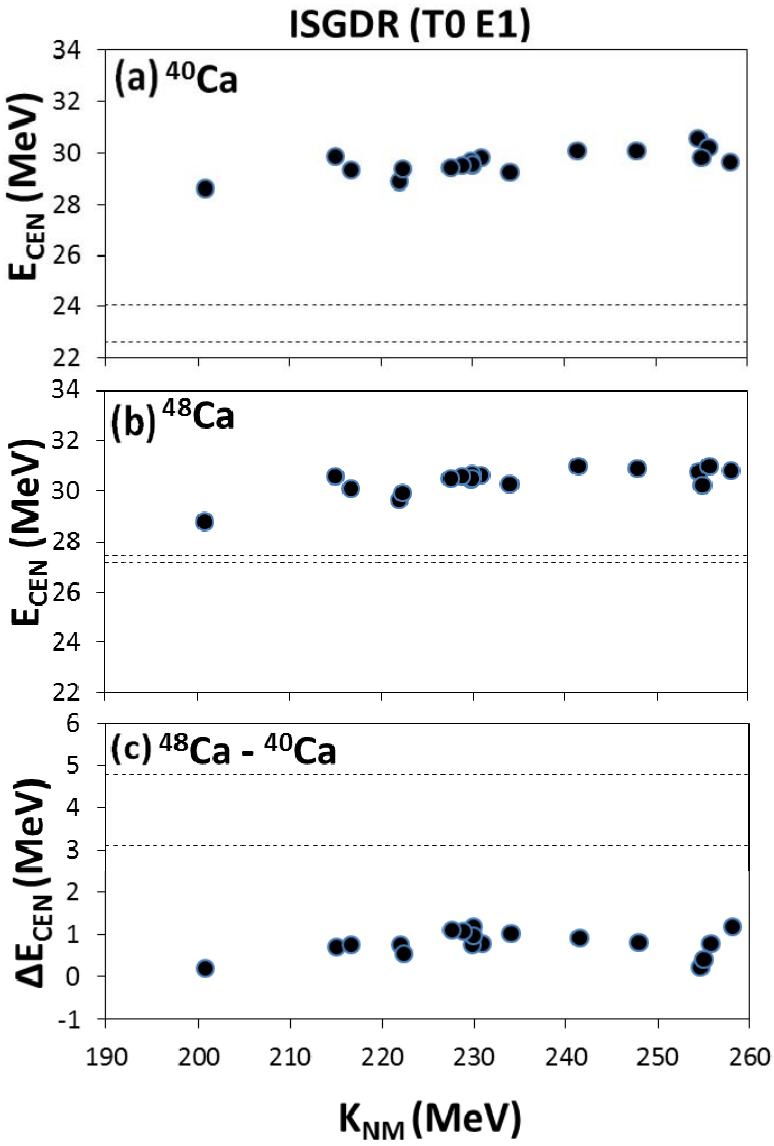

Fig. 10. Same as Fig. 7 except for the ISGDR as a function of K_{NM}..

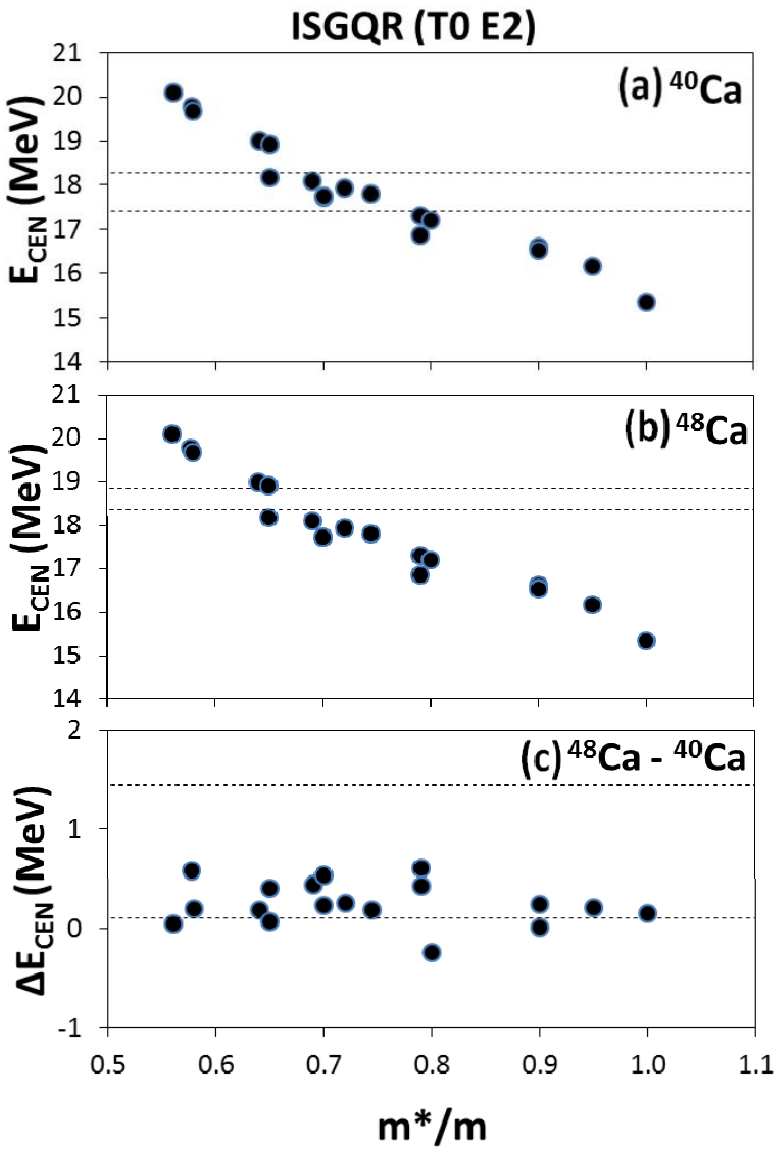

Fig. 11. Same as Fig. 7 except for the ISGQR as a function of m*/m.

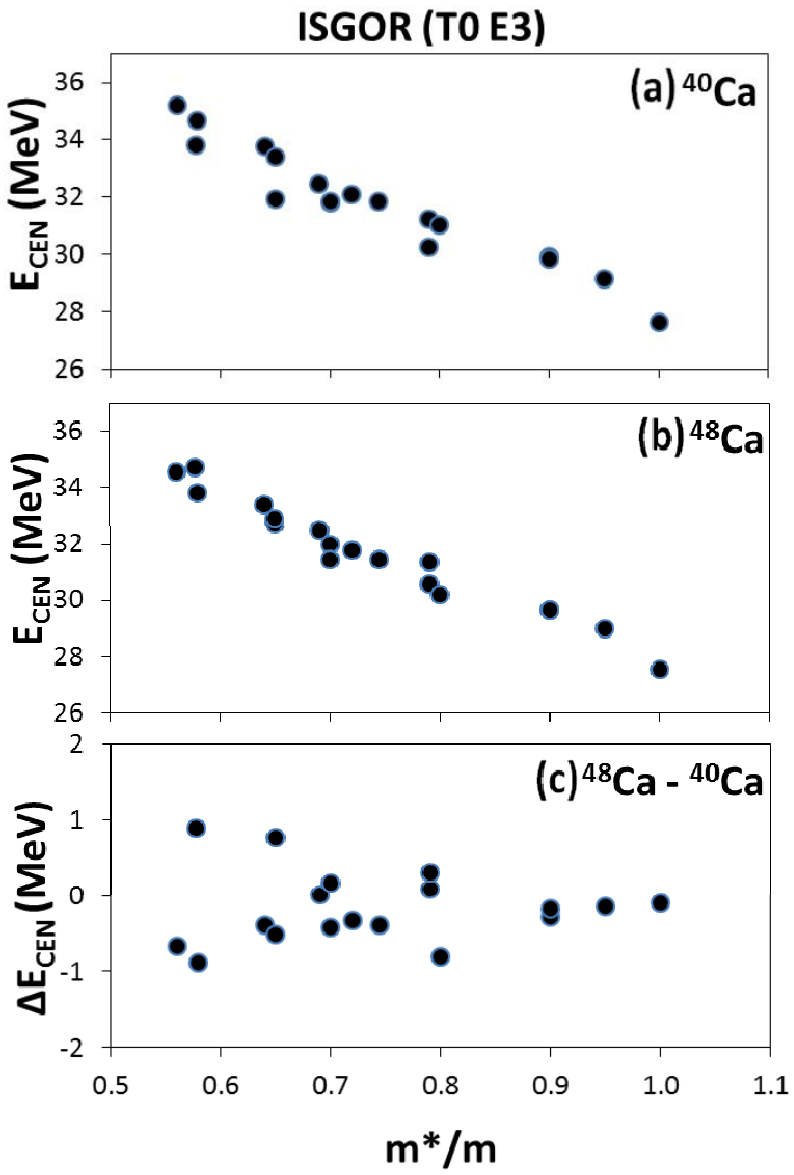

Fig. 12. Same as Fig. 11 except for the ISGOR.

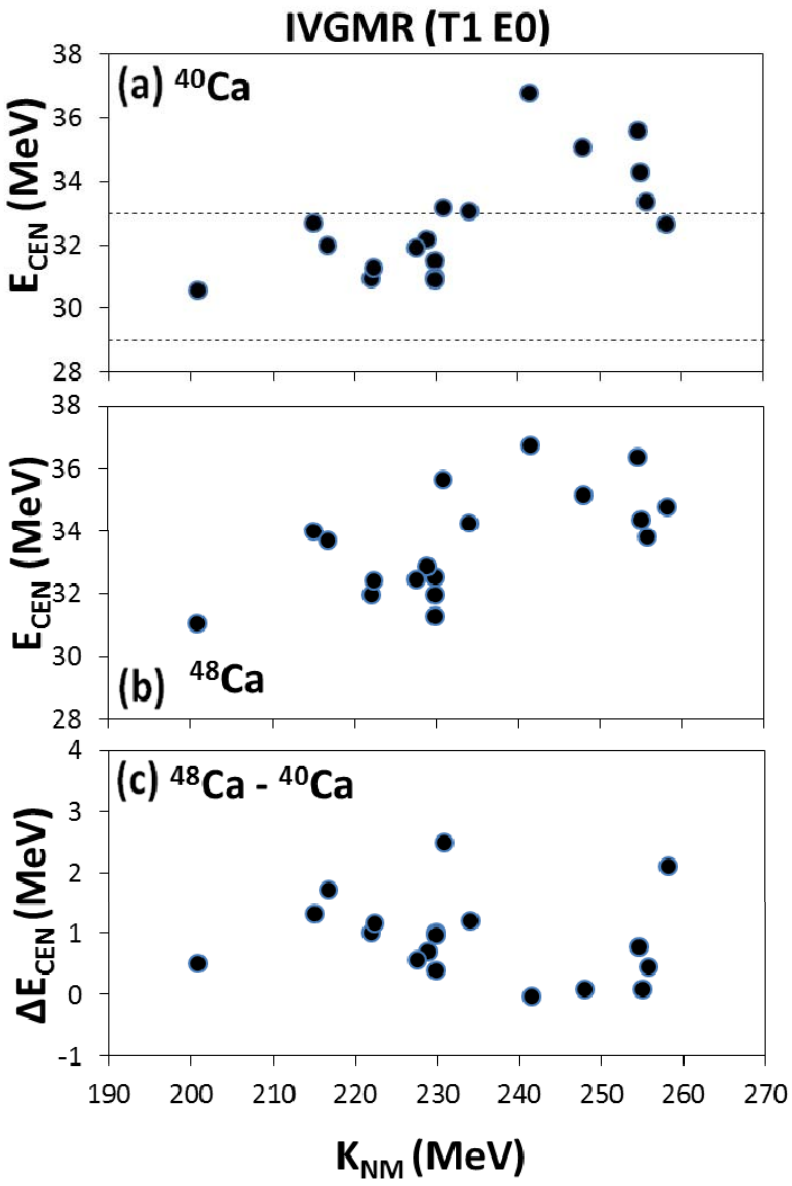

Fig. 13. Same as Fig. 7 except for the IVGMR as a function of K_{NM}. The experimental data is taken from Ref. [10,47].

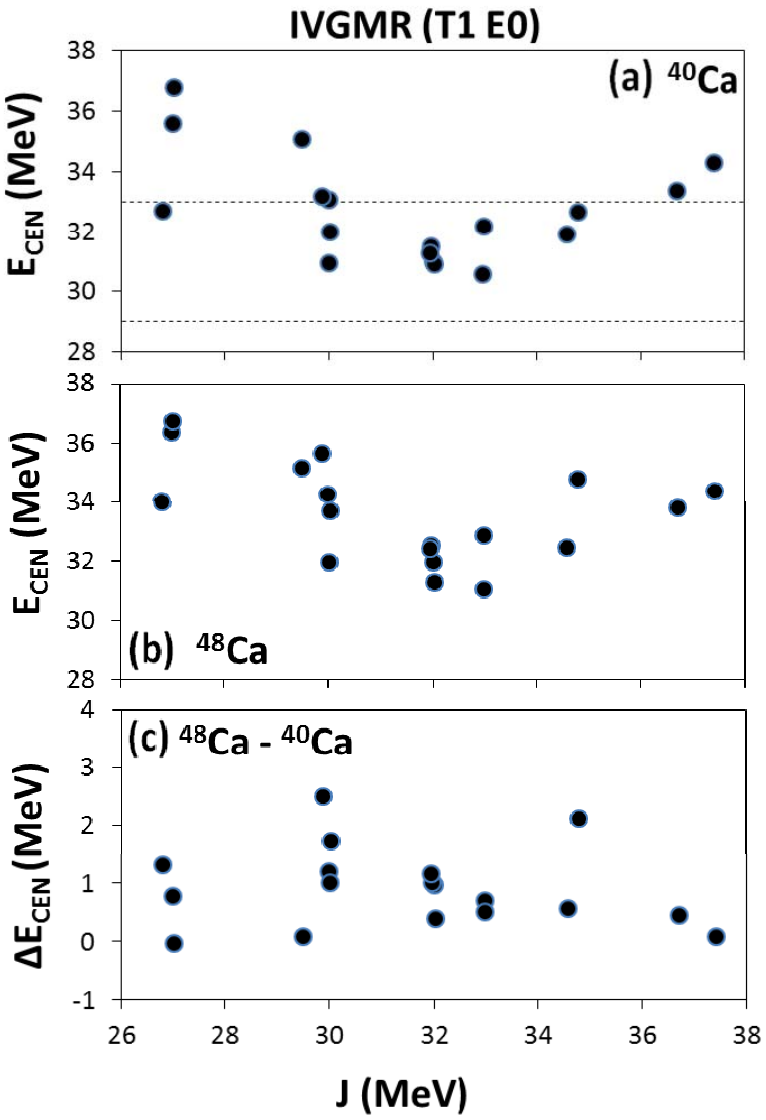

Fig. 14. Same as Fig. 13 except as a function of J.

.

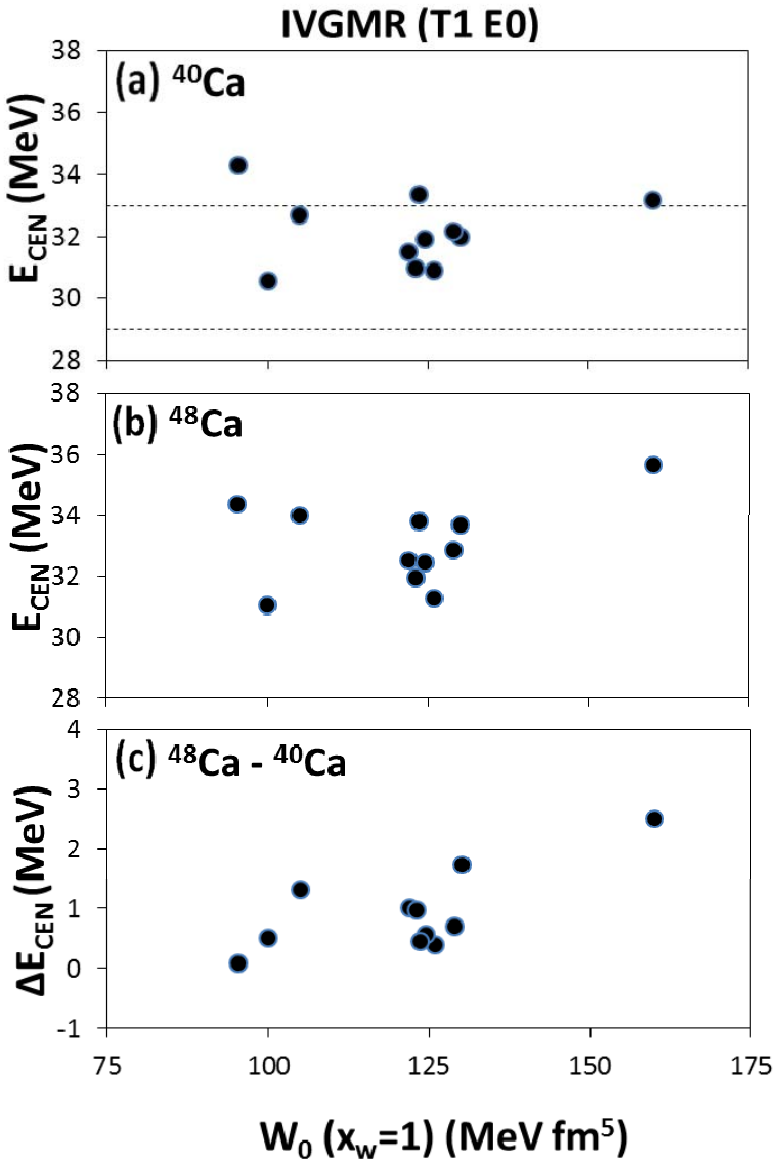

Fig. 15. Same as Fig. 13 except as a function of W_0.

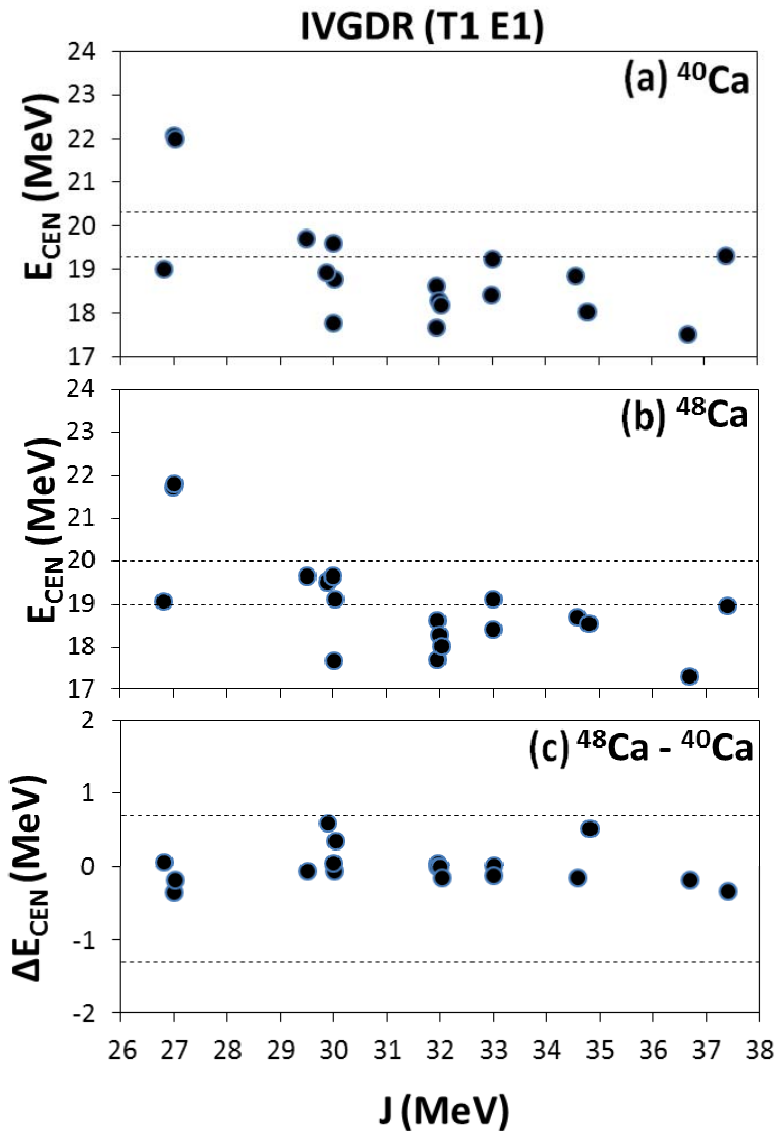

Fig. 16. Same as Fig. 7 except for the IVGDR. The experimental data is taken from Refs. [48,49,50].

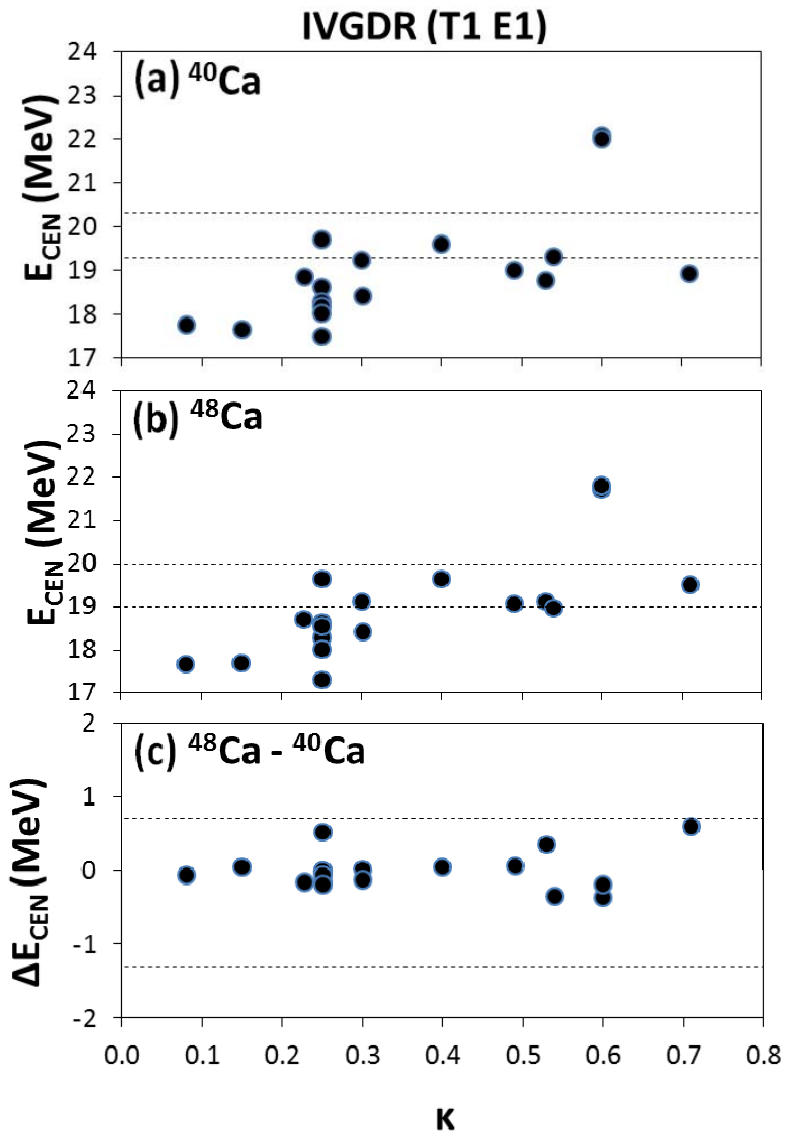

Fig. 17. Similar to Fig. 16 as a function of κ.

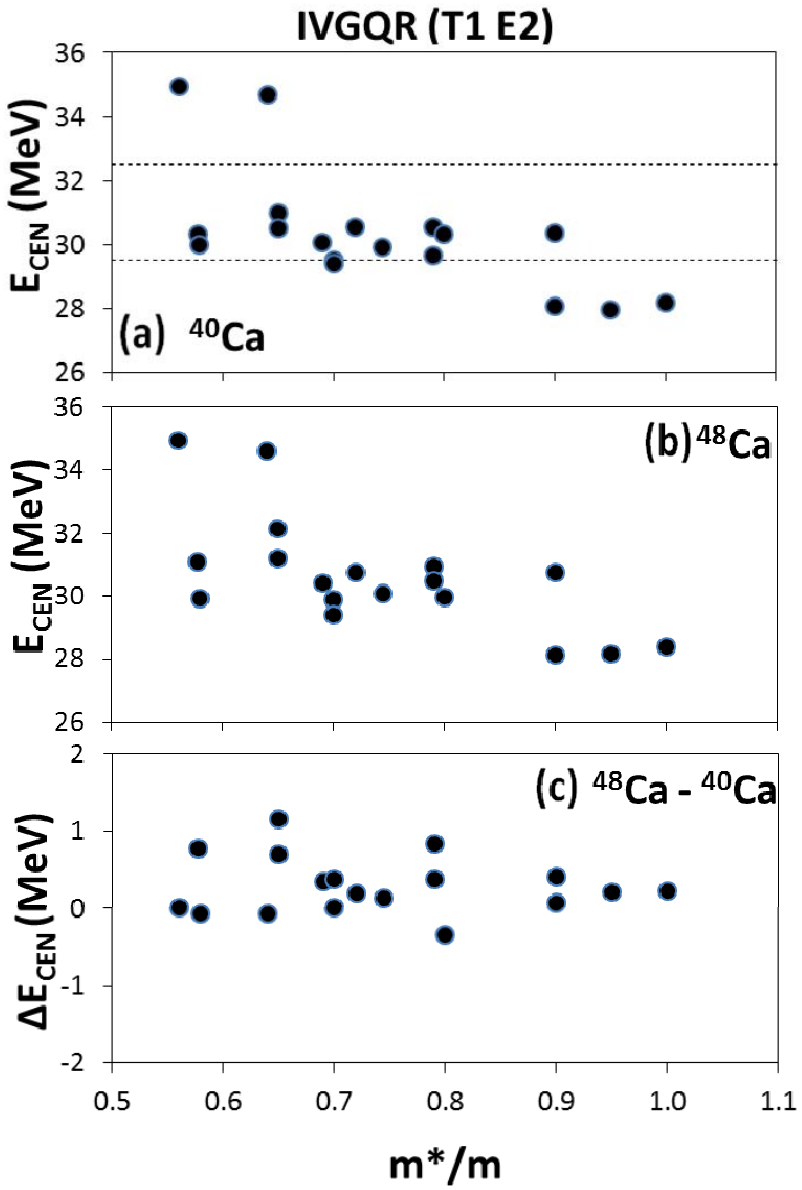

Fig. 18. Same as Fig. 11 except for the IVGQR. The experimental data is taken from Ref. [51].

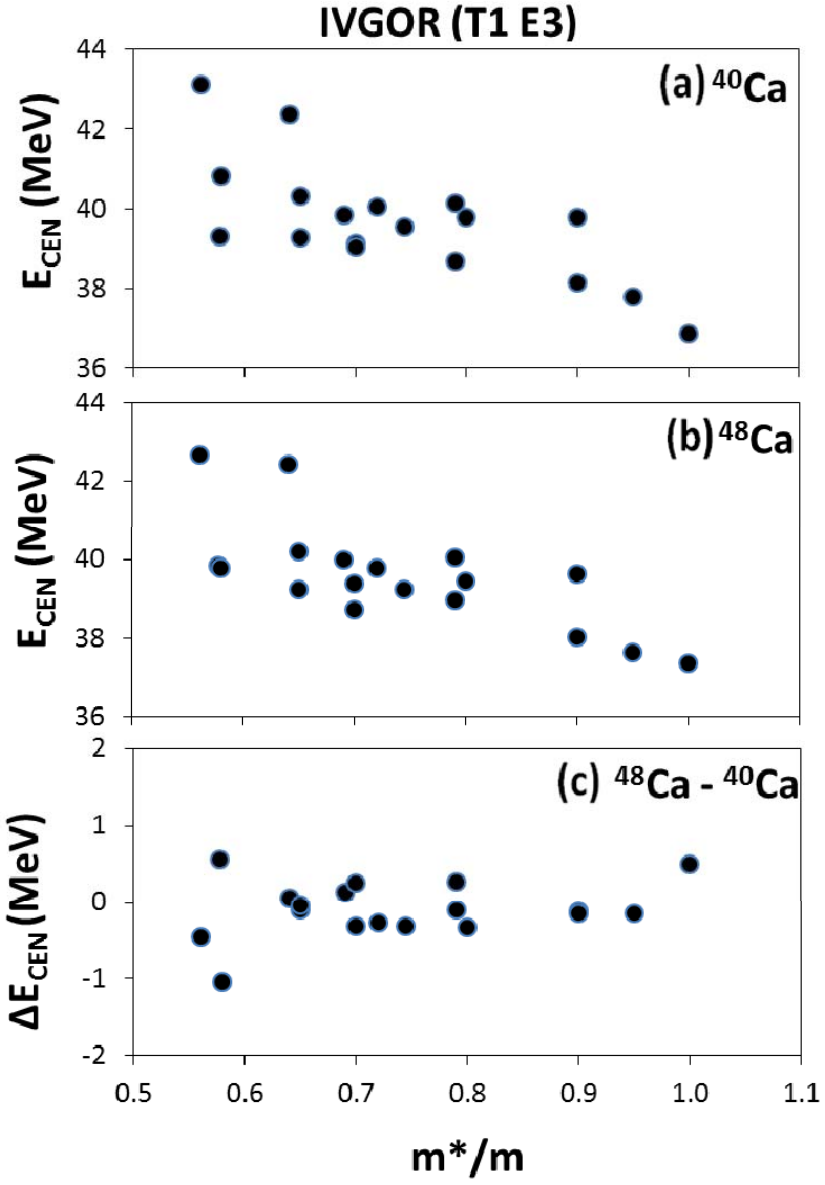

Fig. 19. Same as Fig. 18 except for the IVGOR.